A Synthesis of Hybrid Computational Fluid Dynamics Results for F-16XL Aircraft Aerodynamics

James M. Luckring[1], Michael A. Park[2]
NASA Langley Research Center, Hampton, VA, 23681, USA

Stephan M. Hitzel[3]
Airbus Defense and Space, Military Aircraft, Manching, Germany

Adam Jirásek[4]
The Swedish Defence Research Agency FOI, Stockholm, Sweden

Andrew J. Lofthouse[5]
United States Air Force Academy, Colorado Springs, CO, 80840, USA

Scott A. Morton[6], David R. McDaniel[7]
DoD HPCMP/CREATE Kestrel Team, Eglin AFB, FL 32542, USA

Arthur Rizzi[8],
Royal Institute of Technology, KTH, Stockholm, Sweden

Maximillian Tomac[9]
FS Dynamics, Stockholm, Sweden

A synthesis is presented of recent numerical predictions for the F-16XL aircraft flowfields and aerodynamics. The computational results were all performed with hybrid RANS/LES formulations, with an emphasis on unsteady flows and subsequent aerodynamics, and results from five computational methods are included. The work was focused on one particular low-speed, high angle-of-attack flight test condition, and comparisons against flight-test data are included.

---

[1] Senior Research Engineer, Configuration Aerodynamics Branch, james.m.luckring@nasa.gov, AIAA Associate Fellow.

[2] Research Scientist, Computational AeroSciences Branch, mike.park@nasa.gov, AIAA Senior Member.

[3] Expert for Aerodynamic Design and Numerical Methods, Flight Physics, stephan.hitzel@airbus.com, AIAA Associate Fellow.

[4] Senior Research Scientist, Department of Systems Technology, adam.jirasek@foi.se, AIAA Senior Member.

[5] Director, High Performance Computing Research Center, andrew.lofthouse@usafa.edu, AIAA Senior Member.

[6] Senior Research Engineer, DoD HPCMP CREATE Program, scott.morton@hpc.mil, AIAA Associate Fellow.

[7] Research Associate Professor, University of Alabama at Birmingham, drmcd@uab.edu, AIAA Senior Member.

[8] Professor, Department of Aeronautical & Vehicle Engineering, rizzi@kth.se, AIAA Associate Fellow.

[9] Engineer, Department of Fluid Dynamics, maximillian.tomac@fsdynamics.se, AIAA Senior Member.

This work represents the third coordinated effort using the F-16XL aircraft, and a unique flight-test data set, to advance our knowledge of slender airframe aerodynamics as well as our capability for predicting these aerodynamics with advanced CFD formulations. The prior efforts were identified as Cranked Arrow Wing Aerodynamics Project International, with the acronyms CAWAPI and CAWAPI-2.

I. Nomenclature

BL	airplane butt line, positive starboard	RANS	Reynolds Averaged Navier Stokes
BL	Baldwin-Lomax turbulence model	Re_{cref}	Reynolds number based on c_{ref}, $U\,c_{ref}\,/\,\nu$
$b/2_{ref}$	reference wing semispan	s	local semispan
CFD	Computational Fluid Dynamics	SA	Spalart-Almaris turbulence model
C_p	pressure coefficient	SARC	SA model with rotation correction
c, c_{local}	wing chord	SAS	Scale Adaptive System turbulence model
c_{ref}	reference chord	SD	standard deviation
DDES	Delayed Detached Eddy Simulation	U	free stream reference velocity
DES	Detached Eddy Simulation	URANS	Unsteady RANS
EARSM	Explicit Algebraic Reynolds Stress Model	x,y,z	body-axis Cartesian coordinates
FC	Flight Condition	x_{cp}	longitudinal center of pressure
FS	airplane fuselage station, positive aft	α	angle of attack, deg.
L_{ref}	longitudinal reference length	β	angle of sideslip, deg.
LES	Large Eddy Simulation	Δt^*	nondimensional time step, $\Delta t\,U\,/c_{ref}$
M	Mach number	μ	viscosity
MRP	Moment Reference Point	ν	kinematic viscosity, μ/ρ
n_t	number of physical time steps for statistics	ρ	density

Organizations

ADS	Airbus Defense & Space, Military Aircraft, *Germany*
CAWAPI	Cranked Arrow Wing Aerodynamics Project, International
CREATE	Computational Research & Engineering Acquisition Tools & Environments
DLR	German Aerospace Center, *Germany*
FOI	Swedish Defense Research Agency, *Sweden*
KTH	Royal Institute of Technology, *Sweden*
LaRC	Langley Research Center, *USA*
NASA	National Aeronautics and Space Administration, *USA*
NATO	North Atlantic Treaty Organization
RTO	Research and Technology Organization
USAFA	United States Air Force Academy, *USA*

II. Introduction

Slender airframes present many unique challenges for aerodynamic design and analysis. Although vehicle shaping is heavily influenced by efficient supersonic performance, acceptable transonic cruise and low-speed handling properties must also be accomplished. The development of an efficient supersonic commercial transport has been an elusive challenge, and with the exception of the Concorde, slender aircraft have been developed within the military sector. Despite the growing use of Computational Fluid Dynamics (CFD) for aircraft

development, there are few opportunities to assess how well the CFD methods predict slender-wing aerodynamics, especially at flight conditions.

To partially meet this need, Lamar[1] [2001] created and led a project in the 1990s to obtain flight measurements using an F-16XL aircraft. This project, known as the Cranked Arrow Wing Aerodynamics Project, or CAWAP, produced a unique flight data set that included wing pressures, boundary-layer profiles, and flow visualizations among other quantities. Data were obtained over a broad range of flight conditions (e.g., $0.24 < M < 1.3$, $2.3° < \alpha < 20°$). Initial CFD predictions by Lamar[2] [2003] were less than satisfactory, and an international collaborative program was established to advance our understanding and predictive capability for some of the F-16XL flight conditions. This project, CAWAPI, was facilitated through the NATO Research and Technology Organization (RTO) as task group AVT-113. An overview of this program has been given by Obara and Lamar[3] [2009].

Considerable progress was made in the course of the CAWAPI project for CFD predictions of the flight data, especially at moderate angles of attack and moderate subsonic Mach numbers, and a summary has been given by Rizzi[4] et al. [2009]. However, two flight conditions were identified for which no CAWAPI participants produced acceptable CFD prediction: (i) a low-speed, high angle-of-attack case and (ii) a high-speed (transonic) low angle-of-attack case. Both of these conditions are important to practical operation of high-speed slender aircraft.

These two challenge cases became the focus of a second international collaborative effort, CAWAPI-2. Topics addressed under CAWAPI-2 included improved and denser grid effects, flow modeling effects (e.g., turbulence models), and aircraft modeling factors, such as aeroelastic distortion and control-surface deflections. The work contributed further improvement to our understanding of, and predictive capability for these flows. Progress from this program has been reported by Rizzi and Luckring[5] [2014]. Another outcome from CAWAPI-2 was identification of the apparent need for advanced unsteady CFD modeling, specifically for the low-speed, high angle-of-attack challenge case. This led to the present effort.

The present effort (CAWAPI-3) is focused on the assessment of hybrid RANS/LES modeling for predicting the low-speed, high angle-of-attack case from the previous studies. This particular case, identified as FC-25, has $M = 0.242$, $Re_{cref} = 32.22 \times 10^6$, and $\alpha = 19.84°$. Five studies[6-10] were published in this special session entitled "Hybrid CFD Method Assessments for F-16XL Aircraft Aerodynamics," and five numerical formulations were used. This paper presents a synthesis of those individual findings. Related work from one of the methods was also published by Elmiligui[11] et al. [2015].

The rest of the paper is organized as follows: Section III presents a brief summary of some F-16XL characteristics; Section IV summarizes the numerical modeling used in the current effort; and Section V presents the comparisons among the computed results. Concluding remarks and some acknowledgments are also included.

III. F-16XL Characteristics

The F-16XL was developed from the F-16A aircraft, and a three-view drawing of the F-16XL aircraft is shown in **Figure 1**. Perhaps the most notable feature of this aircraft was the cranked-arrow wing that resulted from a variety of design objectives, not the least of which was efficient supersonic cruise. The wing had an inboard leading-edge sweep of 70° and an outboard leading-edge sweep of 50°. The wing leading edge was interfaced with the fuselage with an S-shaped blending region. An airdam (vertical fence) was situated on the wing upper surface upstream of an actuator pod and slightly inboard the spanstation where the leading-edge sweep changes
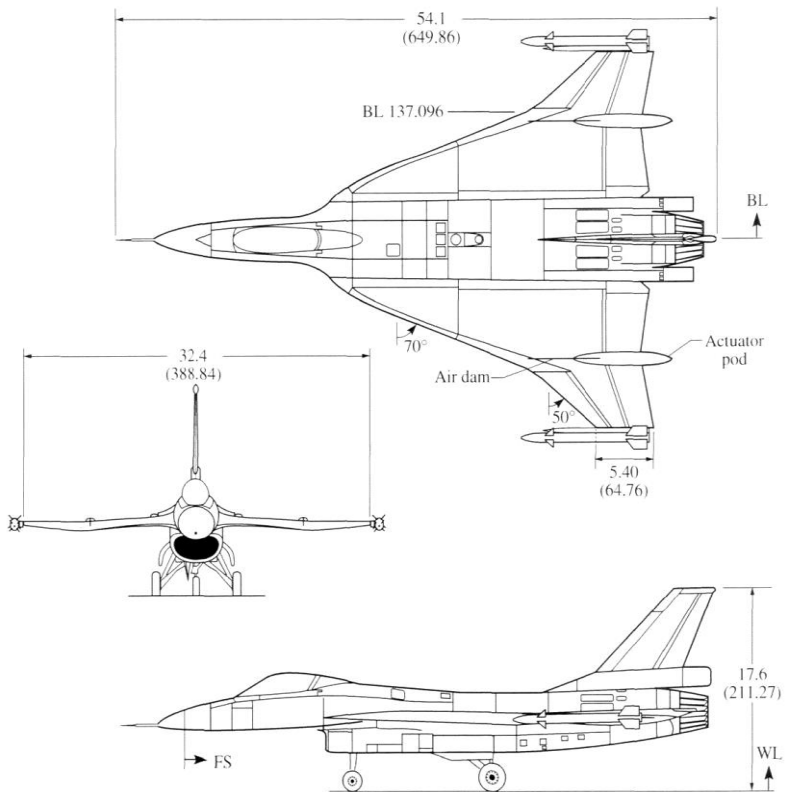
Figure 1. F-16XL overall dimensions.

from 70° to 50°. This slender wing had an aspect ratio of approximately 1.75, and an exposed taper ratio, without the tip rail and missile system, of approximately 0.17. The wing was also very thin, with leading-edge radii that in general were less than 0.10 percent of the wing reference chord. Some summary reference quantities are shown in **Table 1**.

All of these features contributed to the success of this aircraft in meeting the aggregate design objectives of the program, even though the F-16XL never went into full scale production. One of the F-16XL program objectives was to transfer supersonic cruise technology from the commercial to the military sector. As such, the wing captures many high-speed aerodynamic attributes that differ significantly from wings designed for lower-speed performance and that relate to supersonic commercial transports. Additional details of the F-16XL aircraft development, and subsequent flight-test program, can be found in Hillaker[12] [1983] and Talty[13] [1988].

Table 1. F-16XL reference quantities.

$b/2_{ref}$	16.202 ft.	194.42 in.
c_{ref}	24.70 ft.	296.40 in.
L_{ref}	54.16 ft.	649.86 in.
S_{ref} (full span)	600 ft.^{2}	86400 in.^{2}
MRP (x,y,z)	(27.238, 0, 6.338) ft.	(326.86, 0, 76.06) in.

Two prototype aircraft were fabricated, and these were provided to NASA for further flight test research. A photograph of the F-16XL-1 aircraft is shown in **Figure 2**. This is the aircraft used for the CAWAP flight-test program. This program included measurement of wing surface pressures along a number of chordwise butt lines (constant span station) and along a number of spanwise fuselage stations (constant longitudinal station). These stations are


Figure 2. F-16XL-1 aircraft.

shown in **Figure 3.** The Butt Line (BL) and Fuselage Station (FS) numbers that are shown in Figure 3 correspond to distances, in inches, outboard (BL) or aft (FS) of the reference locations shown in Figure 1. Comparisons among the computed results will be presented at a number of these stations, along with the in-flight measurements.

For the low-speed, high angle-of-attack focus of the present work, the outboard panel, with 50° leading-edge sweep, was anticipated to have the most significant unsteady effects. The outer butt lines and outboard portions of

the aft fuselage stations will be examined in this light. Selected correlations at the more inboard and upstream stations will also be included.
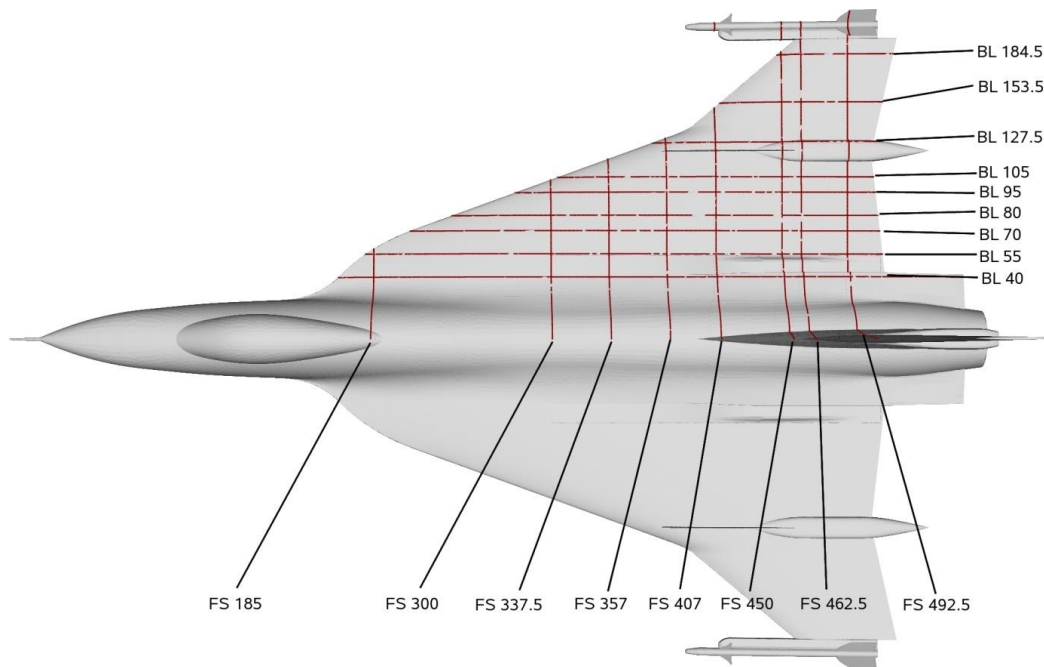
Figure 3. F-16XL spanwise Fuselage Stations and chordwise Butt Lines along which surface pressures were measured.

IV. Numerical Modeling

A. Methods

All of the methods used in the present study incorporate various forms of hybrid RANS/LES modeling, all hybrid results were time accurate, and all of the results were obtained with various forms of unstructured meshes.

The codes used for these studies are DLR-Tau[14], EDGE[15-16], FUN3D[17], USM3D[18-19], and Kestrel[20-22]. All of these codes are well vetted with established user communities, although the hybrid RANS/LES capability is relatively new to EDGE and USM3D. Additional details of the codes can be found among the individual application papers[6-11] of this study. As part of the approach to this study, all partners followed their internal best-practice guidelines. Details for modeling effects studies (e.g., grids, hybrid formulations) and aerodynamic assessments (e.g., Mach or angle of attack effects) were at the participant's discretion, although each participant was asked to provide their preferred modeling solution at a common condition for comparison purposes.

B. F-16XL Modeling

The focus condition for the hybrid RANS/LES modeling was FC-25, which has M= 0.242, Re_{cref} = 32.22 x 10^6, α = 19.84°, and β = 0.7°. For comparisons among the numerical methods, it was decided among the participants to set the sideslip angle β to zero degrees in order to allow for half-span computations and analysis. Analysis of sideslip effects, including values on the order of $\pm$ 5°, have been given by Hitzel[23] [2014].

Because this F-16XL work was focused on flight data, propulsion effects have to be included. FC-25 was one of the CAWAP flight conditions for which measurements were taken to guide propulsion boundary conditions for the CFD simulations. A summary of the FC-25 propulsion conditions is shown in

Table 2. Propulsion conditions, FC 25.

Altitude	10,000 ft.
Inlet static temperature	470.1 °R
Inlet static pressure	8.72 psia
Inlet velocity	474.8 ft./sec
Inlet Mach number	0.447
Exit total temperature	1209 °R
Exit total pressure	26.3 psia

Table 2. The propulsion boundary-condition approach developed in the CAWAPI work was used in the present work, and all participants used the same propulsion simulation approach to develop propulsion boundary condition consistent with their code.

A summary of the modeling approaches and assessments is shown in **Table 3**. For cases where multiple hybrid RANS/LES approaches were studied, the participant's preferred approach is indicated in italics and red. Some general observations from this collective work are:

- Three partners included a contrast between RANS and hybrid RANS/LES formulations

- Two partners contrasted the hybrid approach

- One partner included a time-step assessment

- Three partners included grid resolution studies

- Four partners worked with adaptive grids

- Two partners included adaptive grid assessments

Table 3. RANS and Hybrid RANS/LES methods details.

Partner	Code	RANS	Hybrid RANS/LES Flow Modeling	Δt^*	n_t	Grid Size (Semispan)	Grid Adaptation
Airbus	DLR-Tau	None	SAS/DES	0.0063	1500	45.0 M nodes	Manual
KTH	EDGE/Hyb0	EARSM, RANS, URANS	BL/DES	0.0005	5000	42.9 M nodes	Manual
NASA LaRC	FUN3D	SA	SA/DES *SARC/MDDES*	0.0010	8000	10.6, *24.3* M nodes	None
NASA LaRC	USM3D	None	SA/DES	*0.0008* 0.0041	*16000* 6000	19.4 M cells	None
CREATE	Kestrel-a	None	SA/DDES	0.0053	5000	NB-21.9, 23.3, 24.4, *29.6*, 31.8 M cells OB-71.4, 88.9, 92.9, *93.1* M nodes	Solution Based, hybrid
USAFA	Kestrel-b	SA, SARC	SA/DDES *SARC/DDES*	0.0053	8000	56.8, 68.8, *86.5*, 89.7 M cells	Solution Based

Some additional comments for the adaptive grid work with Kestrel are warranted. The adaptive mesh refinement approach taken by the CREATE team exercised a hybrid mesh approach available in Kestrel where the near-body (NB) region is modeled with a prismatic unstructured grid and the off-body (OB) region is modeled with a Cartesian unstructured grid. The adaptive mesh refinement approach taken by the USAFA used unstructured prismatic/tetrahedral meshes.

It is also observed that the grids for FUN3D and USM3D are atypically small. In prior CAWAPI-2 RANS work with USM3D, Elmiligui[24] et al. published grid effects results for tetrahedral grids including 19 M, 63 M, and 143 M cells. Their preferred grid had 63 M cells, and the CAWAPI-2 partners collectively averaged 46 M unknowns (i.e., cells or nodes). However, for the present work the two FUN3D grids were in hand, and it was decided to use them and roughly match the larger FUN3D grid size with the small USM3D grid from their previous work.

V.   Comparison of Results

Results among the six numerical simulations will be compared in this section. Overall flowfield images will be compared first. Next, wing surface pressures will be compared for both mean and fluctuating quantities. This will be followed by a field point analysis for the spectral content at four field points above the wing. Finally, mean and fluctuating force and moment properties will be contrasted among the numerical results. Not all participants could generate all results for all comparisons, and yet comparisons shown are still instructive.

A. Flowfield

A standard Q-criterion was adopted for visualizing the vortical flowfields about the F-16XL aircraft. Q is defined as $\mathbf{Q} = (1/2) [\|\mathbf{\Omega}\|^2 - \|\mathbf{S}\|^2]$ where $\mathbf{S}$ and $\mathbf{\Omega}$ are the strain and rotational components of the velocity gradient,

respectively. For comparison purposes, the flows were displayed for a value of $Q = 1 \times 10^{-3}$ colored by pressure coefficient over the range $-2.0 < C_P < 0.2$ (where lower values of Q will bring out more vortical content.) Four partners provided these results. One partner did not have this criterion available and used the standard λ_2 criterion for visualization. λ_2 is the second eigenvalue of the tensor $\mathbf{J} = [\mathbf{\Omega}^2 + \mathbf{S}^2]$, and visualizations were created with $\lambda_2 = -1.0$.

These two criteria, with the chosen threshold values[*], produced images with similar vortical content, and the Q and λ_2 results will be used to illustrate the overall vortical flows for FC-25. A top-view of these flows is shown in **Figure 4** with results from Kestrel-a (Q-criterion) and DLR-Tau (λ_2 criterion). Looking at the Kestrel results, Figure 4a, the dark blue primary vortex from the inner, 70°-swept wing is clearly evident. Slightly outboard of this vortex is a lighter blue vortical structure where a secondary vortex would be expected. Further outboard, and close to the leading edge, a tertiary vortex also seems to be indicated. The secondary and tertiary vortices are small, and not commonly seen as distinctly as in the Kestrel-a results. These small, vortical features may be associated with the Hybrid RANS/LES modeling, the fine-grid resolution of this solution, the high Reynolds numbers of the target condition, and F-16XL geometry. However, numerical effects (including displays) for these small, vortical features need to be assessed, and additional analysis is warranted. The vortices from the 70°-swept wing tear from the leading edge at the break in leading-edge sweep, whereupon the primary vortex appears to burst and the secondary vortex appears to merge with the airdam vortex (both are counter rotating). On the outer, 50°-swept wing panel, a new leading-edge vortex (dark blue) is seen, and further outboard, this vortex merges with several smaller vortical structures from the tip missile.

Many of these features are quite similar in the DLR-Tau results, Figure 4b. Both solutions/displays show fairly coherent vortices upstream on the inner 70°-swept portion of the wing, and both evidence vortex-breakdown patterns for these vortices on the inner, aft portion of the wing. The DLR-Tau results also include visualization of reversed flow in blue, and this further evidences the presence of vortex breakdown. This analysis also indicates that bursting may be occurring slightly upstream of the change in leading-edge sweep. Oblique views of these same
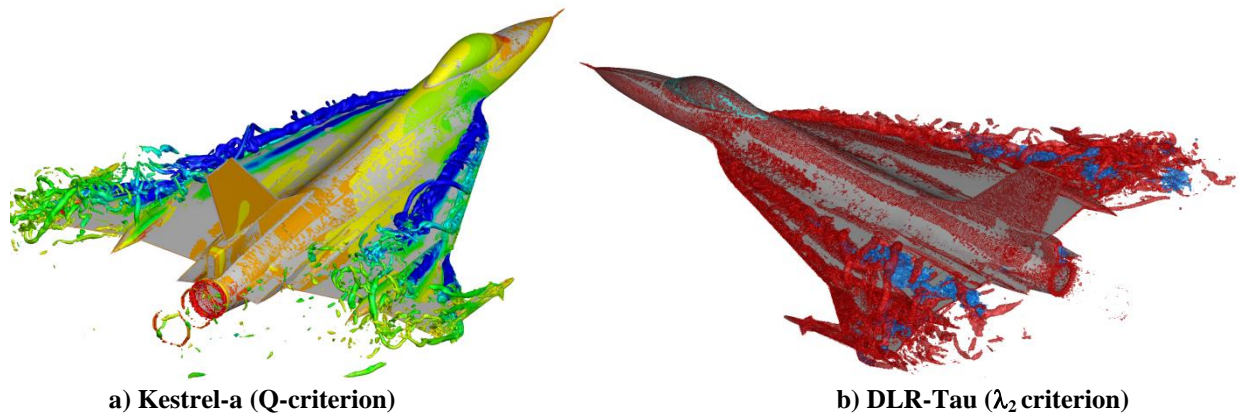
―――――――――――――――

* The display values of Q (Q = 0.001) and λ_2 ($\lambda_2 = -1.0$) correspond with velocities normalized by freestream speed of sound and grids in full-scale inches or full-scale meters, respectively.

solutions are shown in **Figure 5**. The overall features of the vortical flowfields, and even some details, are quite similar between these results, despite the fact that they are from different codes, using different turbulence models and hybrid technology, and that they use different display criteria.

From these flowfields, it is observed that the nature of unsteady vortical flow can be expected to be different on the inboard, upstream and the outboard, downstream portions of the wing. At this macro-scale of analysis, the upstream portion of the wing has a somewhat conventional vortical environment with coherent vorticity. The downstream and outboard portions of the wing include more vortical flow phenomena, such as vortex interactions and vortex breakdown, which also contribute unsteady effects peculiar to these vortical flow physics.

a) Kestrel-a (Q-criterion)

b) DLR-Tau (λ_2 criterion)
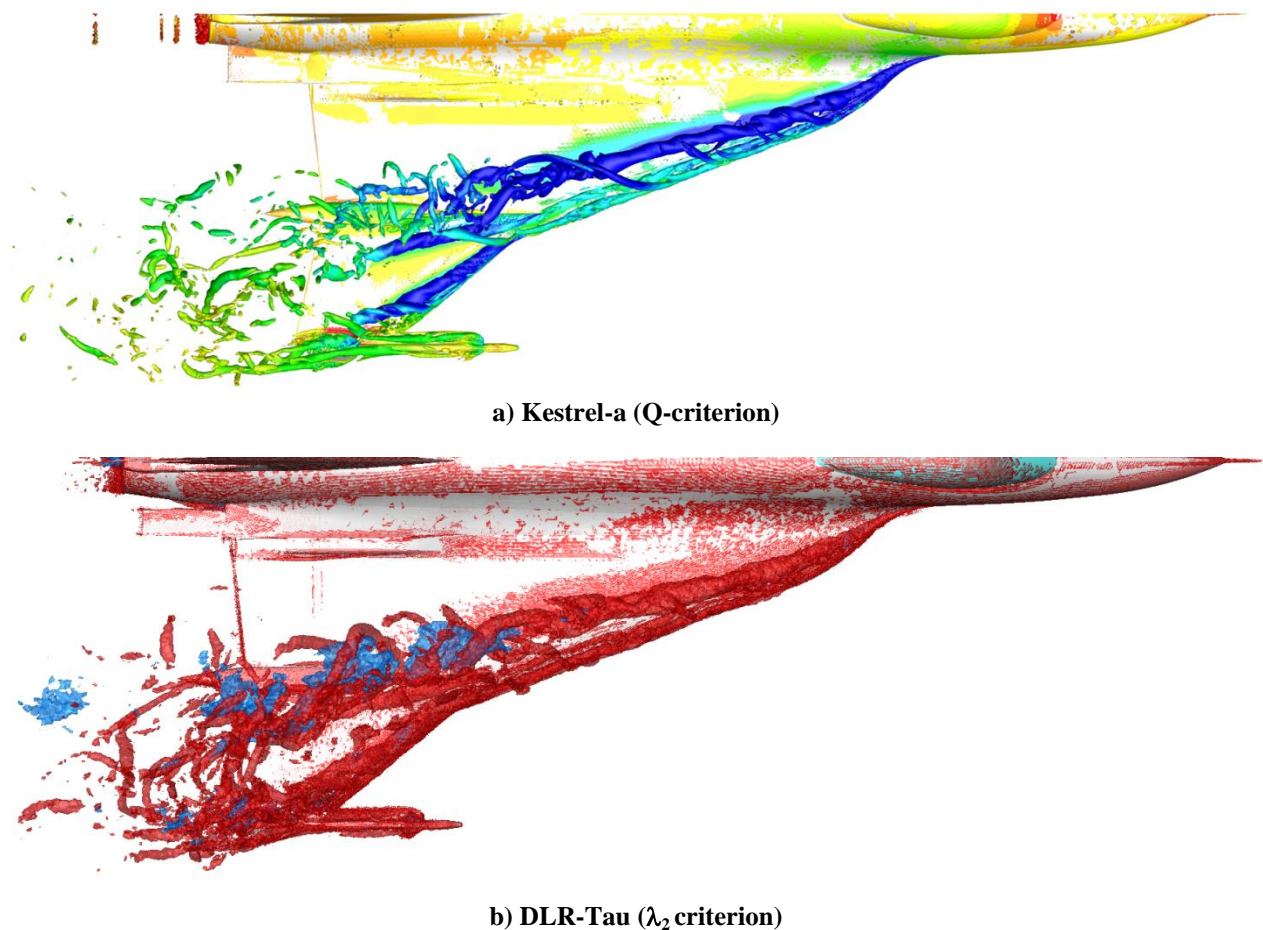
Figure 4. Comparison of off-body flowfields, top view.
FC-25, M = 0.242, Re_{cref} = 32.22 x 10^6, α = 19.84°

**a) Kestrel-a (Q-criterion)**   **b) DLR-Tau (λ_2 criterion)**

Figure 5. Comparison of off-body flowfields, isometric view.
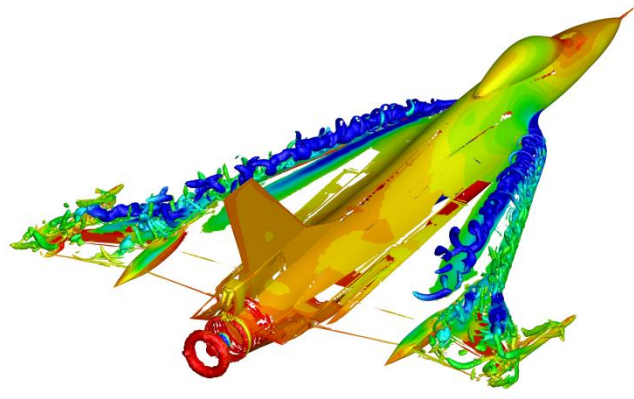**FC-25, M = 0.242, Re_{cref} = 32.22 x 10^6, α = 19.84°.**

Turning now to the other solutions, comparisons among the four results with the Q-criterion are presented in **Figure 6** (isometric view), **Figure 7** (top view), and **Figure 8** (side view). Results are shown for the EDGE, FUN3D, and Kestrel codes. The results from all four simulations have captured the same overall vortical structures just discussed with Figure 4. All four results look similar at the scale shown over the forward, highly-swept portion of the wing. Between the two Kestrel simulations, the Kestrel-b results show more vortical content on the aft portion of the wing.

Grid resolution is one factor affecting these images. The FUN3D results show less vortical content on the aft portion of the wing, and this could be due to the relatively small grids used with these simulations. The Kestrel results had fine grids that were also adapted, and the detail in these images may be due in part to vortical grid resolution. The EDGE results had a moderate grid, and the lack of vortical resolution may be associated with the local grid resolution in the vicinity of the vortices. Additional analysis for local grid resolution of these vortices would be useful.
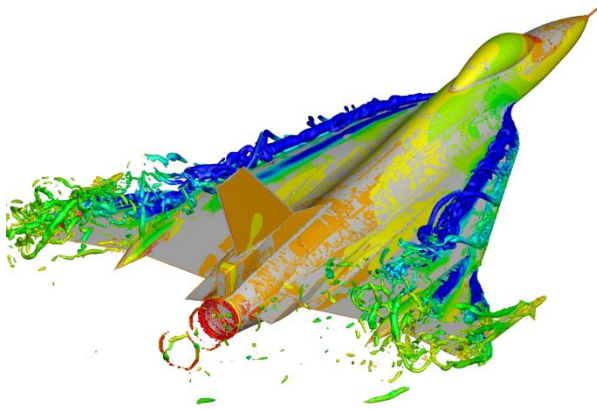
The amount of vortical detail in all these results is limited by the particular Q threshold, Q = 0.001, that was chosen for the common displays, and the individual research papers using EDGE[10] and Kestrel[6,8] include images with higher vortical content.
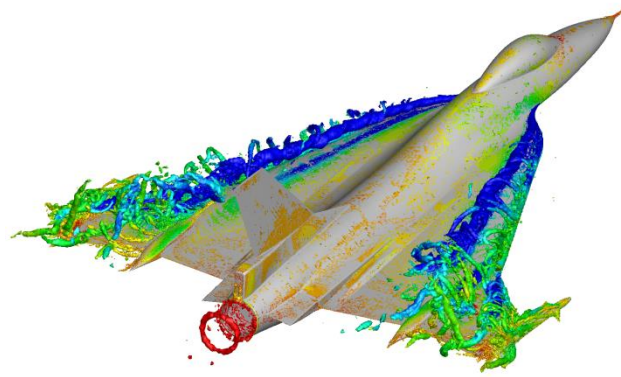
American Institute of Aeronautics and Astronautics
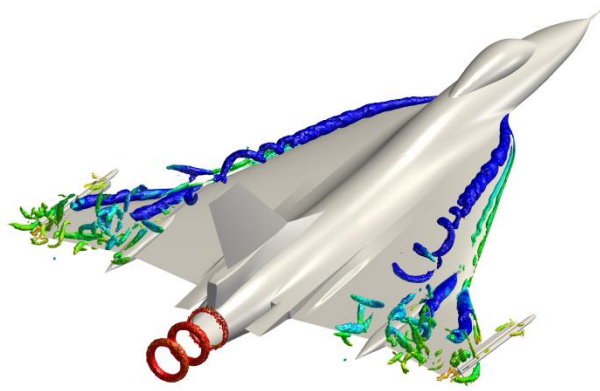
a) EDGE

b) FUN3D

c) Kestrel-a

d) Kestrel-b

Figure 6. Comparison of off-body flowfields, oblique view.
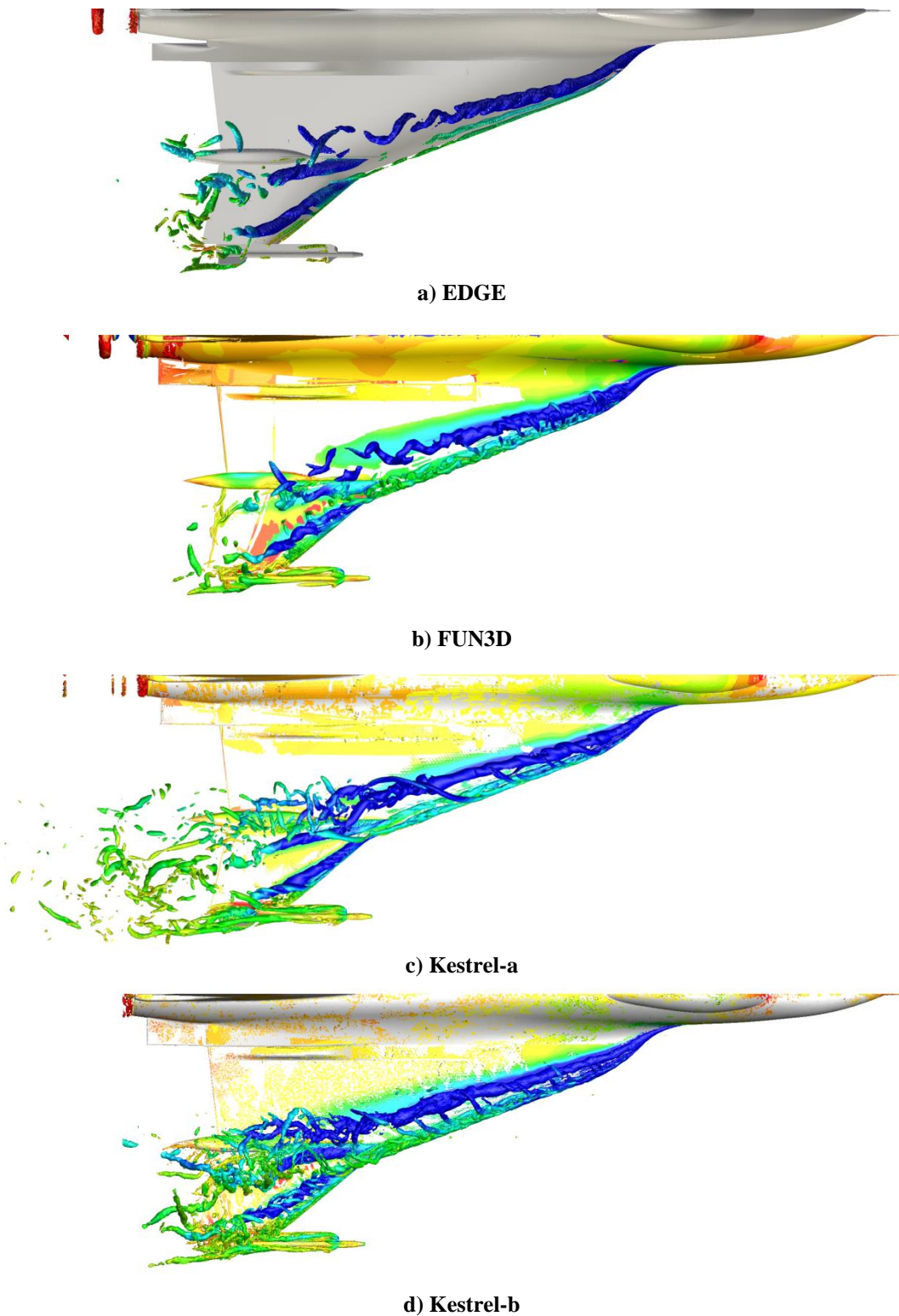**FC-25, M = 0.242, Re$_{cref}$ = 32.22 x 10^6, α = 19.84^o.**

a) EDGE

b) FUN3D

c) Kestrel-a

d) Kestrel-b

Figure 7. Comparison of off-body flowfields, top view. FC-25, M = 0.242, Re$_{cref}$ = 32.22 x 10^6, α = 19.84^o.
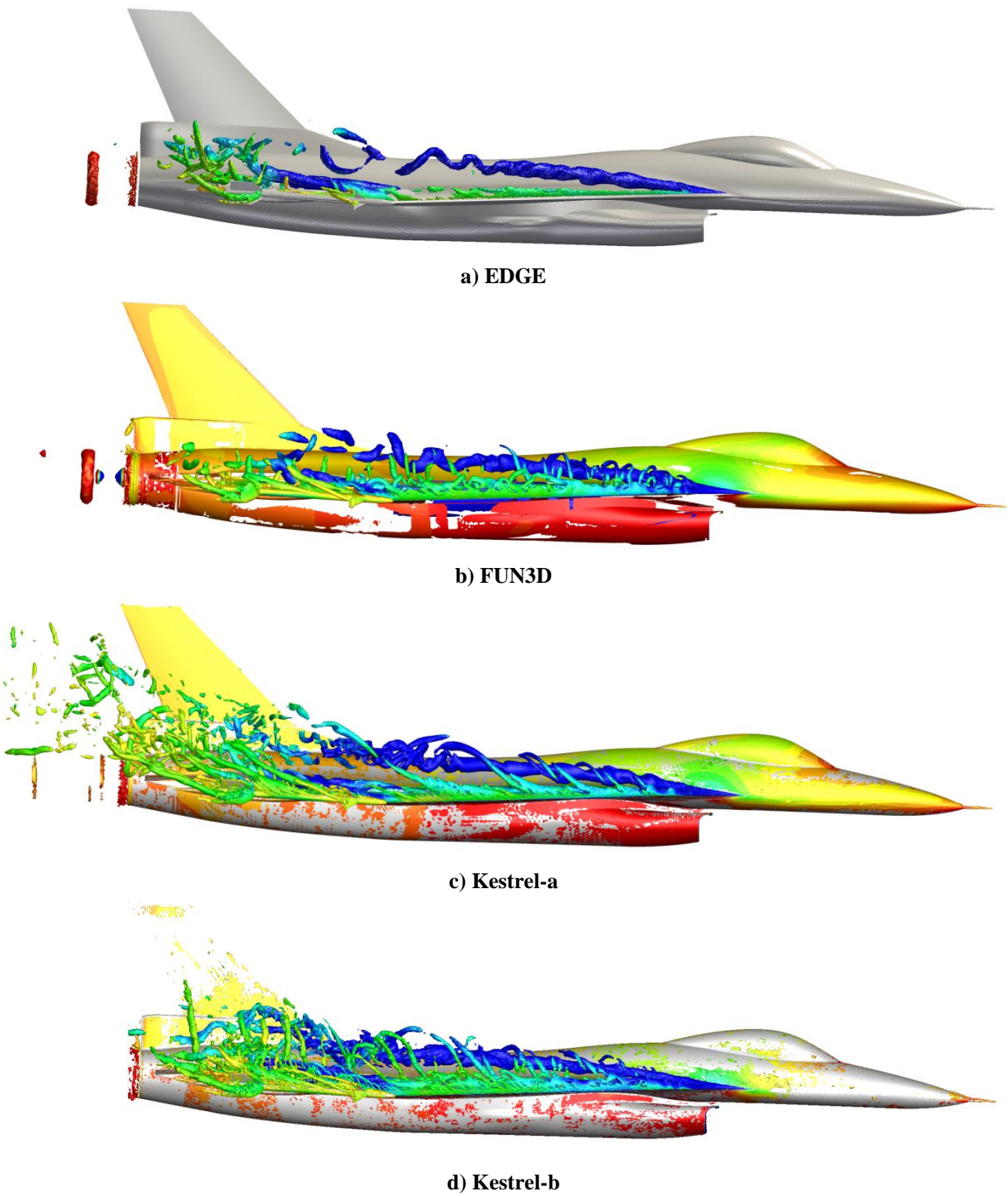
a) EDGE

b) FUN3D

c) Kestrel-a

d) Kestrel-b

Figure 8. Comparison of off-body flowfields, side view. FC-25, M = 0.242, Re_{cref} = 32.22 x 10^6, α = 19.84°.

B. Wing Pressures

A more detailed assessment among the hybrid RANS/LES simulations can be performed by using the wing surface pressure distributions. The same four partners that provided the Q-criterion images provided data for comparison plotting of mean and fluctuating surface pressure coefficients. Fluctuating effects will be shown with distributions of the standard deviation (SD, or one sigma) measure of the local unsteady pressures. The number of time steps used for this statistical processing was included in Table 3 for each method.

Comparisons will be presented first along spanwise fuselage stations followed by chordwise butt lines. The stations chosen coincide with locations for which flight data are available. Flight measurements will be included in these assessments, although only mean pressure quantities were recorded.

1. Spanwise fuselage stations

Results will be presented for FS- 300, 337.5, 375, 407.5, and 450. Comparison among surface pressure distributions are first presented in **Figure 9** for FS-300. Looking at the mean pressure coefficients, Figure 9a, all of the results show a classical leading-edge-vortex suction peak at about 0.75 local semispan. The EDGE and Kestrel-a solutions show a stronger secondary vortex flow at about 0.95 local semispan. Correlation among the results is good as is the correlation with experiment. The fluctuating pressure coefficients, Figure 9b, have two curves for each solution, C_p (mean + SD) and C_p (mean − SD), and the mean flight data are included for reference. Thus, the measure of unsteadiness is the distance between the two curves from any one method. The larger fluctuations are outboard, in the vicinity of the secondary vortex flow, and the unsteady effects are similar among the results shown.

Results are presented in **Figure 10** for FS-337.5. Correlation of mean pressure coefficients among the methods and with the data is still very good. The methods also show less difference in the secondary vortex region at this station than they did at the previous station (FS-300). Unsteady effects now appear to be manifested more in the footprint of the primary vortex. Once again the unsteady effects are similar among the methods.

Results are presented in **Figure 11** for FS-375. This station is slightly upstream of the break in leading-edge sweep and includes the beginning of the vertical fence referred to as an airdam. Looking at the mean pressure coefficients, Figure 11a, the effects of the airdam can be seen at approximately 0.93 of the local semispan. Once again, the correlation among the computed results and the experiment is quite good at this fuselage station. The unsteady effects, Figure 11b, are once again manifested under the primary leading-edge vortex and persist outboard. The unsteady effects are very similar among the results shown.

Results are presented in **Figure 12** for FS-407.5. This station is slightly downstream of the break in leading-edge sweep. Correlation among the methods, and with experiment, for the mean pressure coefficients is quite good. The spanwise trends outboard of the airdam are now quite different from upstream stations and warrant some explanation. The airdam is a streamwise vertical plate with an aerodynamically sharp leading edge along its top. The spanwise flow induced by the leading-edge vortex from the inboard 70° leading edge creates an airdam primary vortex separating from its leading edge; this primary vortex results in the suction peak observed at about 0.86 local semispan. It must also be commented that the airdam primary vortex is counter-rotating to the traditional sense. Further outboard, a third suction peak is observed, especially in the Kestrel-a results, that is due to the leading-edge vortex forming from the outer-panel, 50°-swept leading edge. The other solutions are only beginning to show evidence of this vortex. Inboard of the airdam, the unsteady pressure coefficients, Figure 12b, are similar to the previous fuselage station. However, outboard of the airdam, the level of unsteadiness is increased as compared to the previous station. Unsteadiness in the airdam vortex is comparable among the methods shown. For the outboard leading-edge vortex, Kestrel-a showed the largest unsteadiness, perhaps in association with the stronger vortex of that simulation. The remaining methods produced similar levels of unsteadiness for this vortex.

Results are presented in **Figure 13** for the last fuselage station, FS-450. This station is slightly ahead of the leading-edge/missile-rail juncture. Correlations among the methods and with experiment, for the mean pressure coefficient, inboard of the airdam are good. However, outboard of the airdam there is quite a bit of scatter among the methods. This outboard portion of the wing is also where the greatest unsteadiness is shown, Figure 13b. This increased unsteadiness on the outer panel will also be addressed in the analysis of the chordwise butt lines presented next.
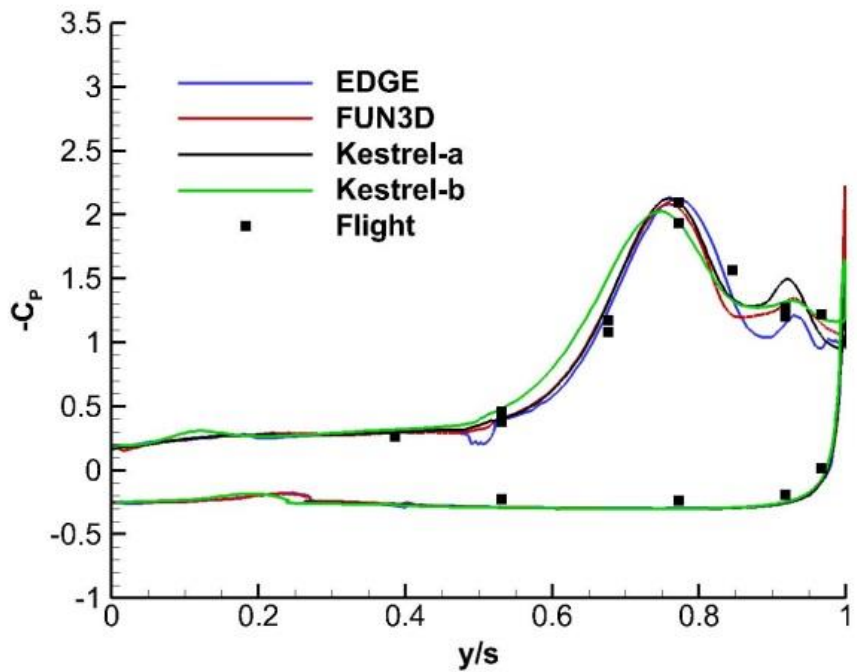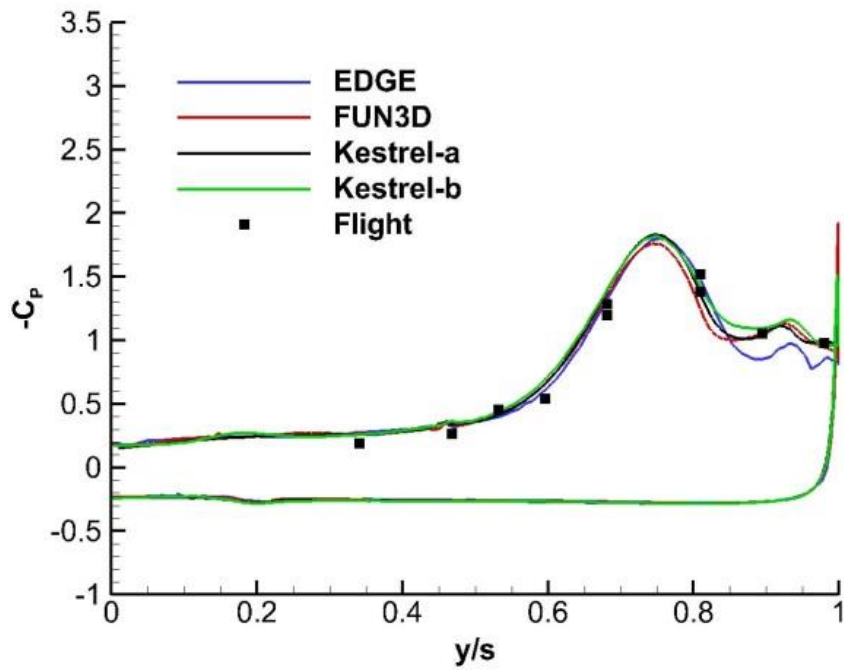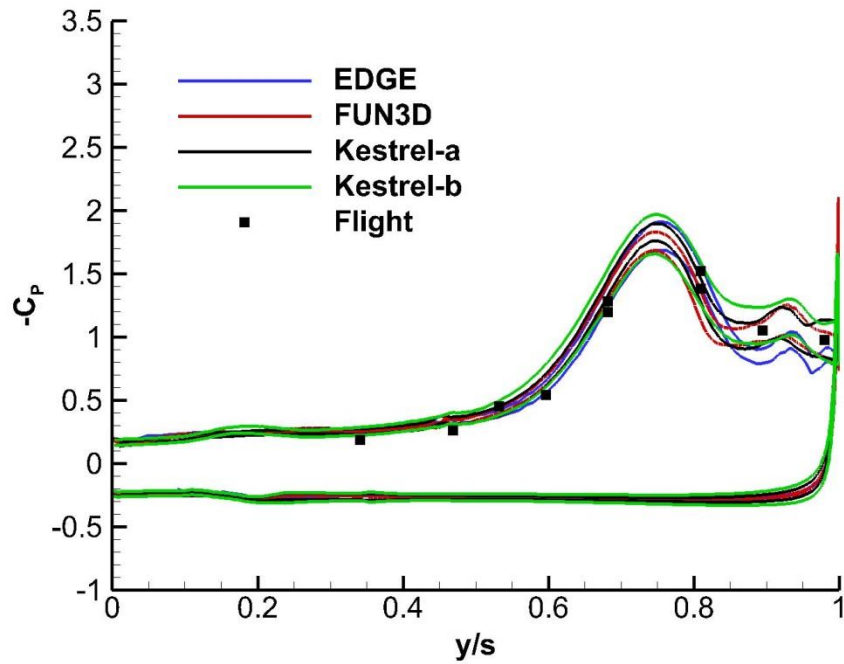
a) Mean C_p
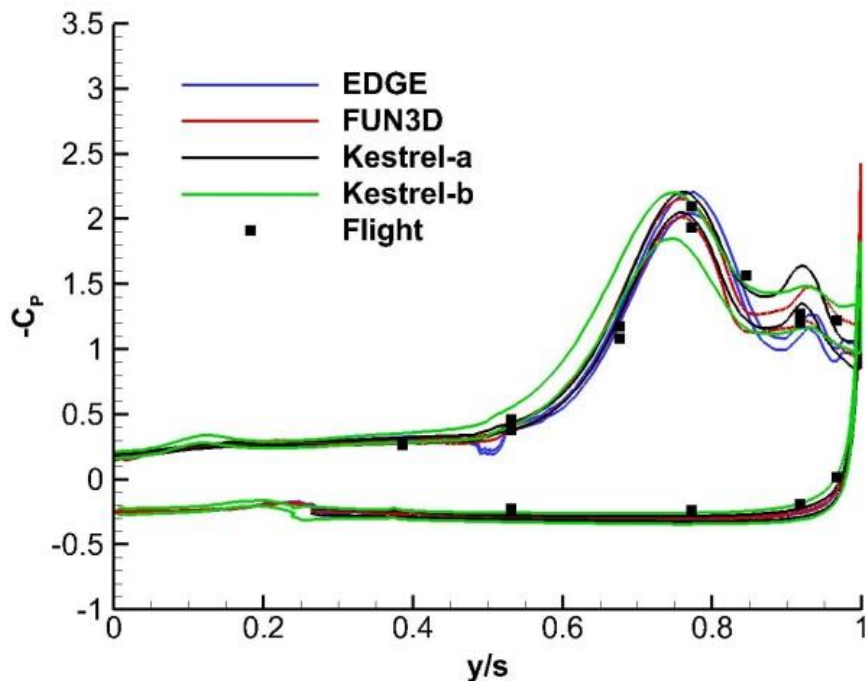
b) Mean ± SD C_p

Figure 9. Unsteady surface pressure coefficients, FS-300. FC-25, M = 0.242, Re_{cref} = 32.22 x 10^6, α = 19.84°.
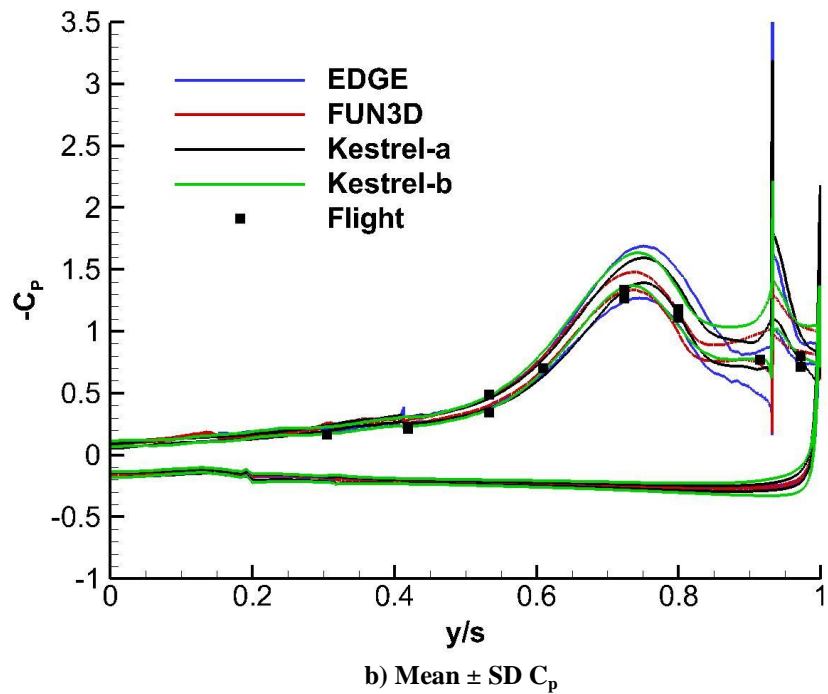
a) Mean C_p

b) Mean ± SD C_p

Figure 10. Unsteady surface pressure coefficients, FS-337.5. FC-25, M = 0.242, Re_{cref} = 32.22 x 10^6, α = 19.84°.

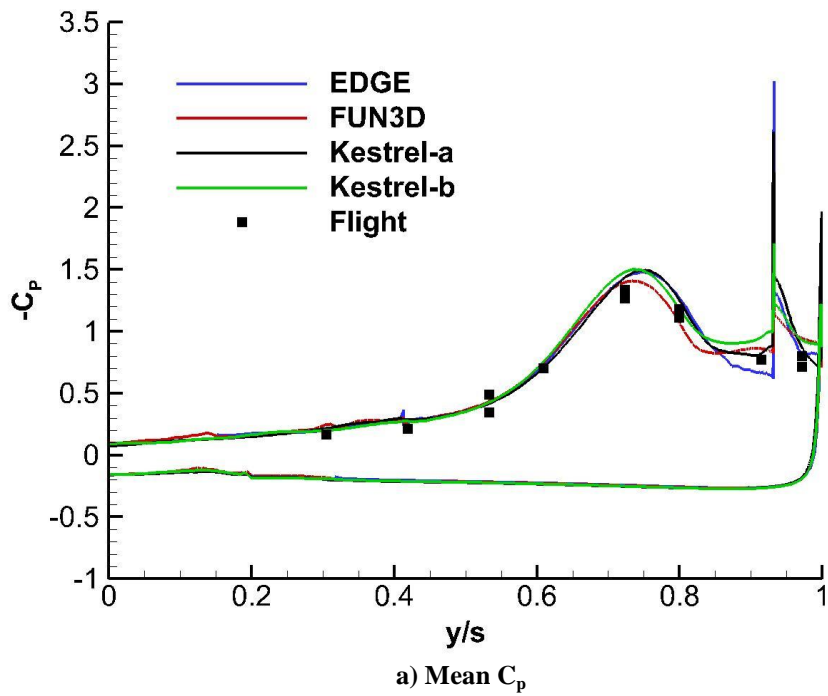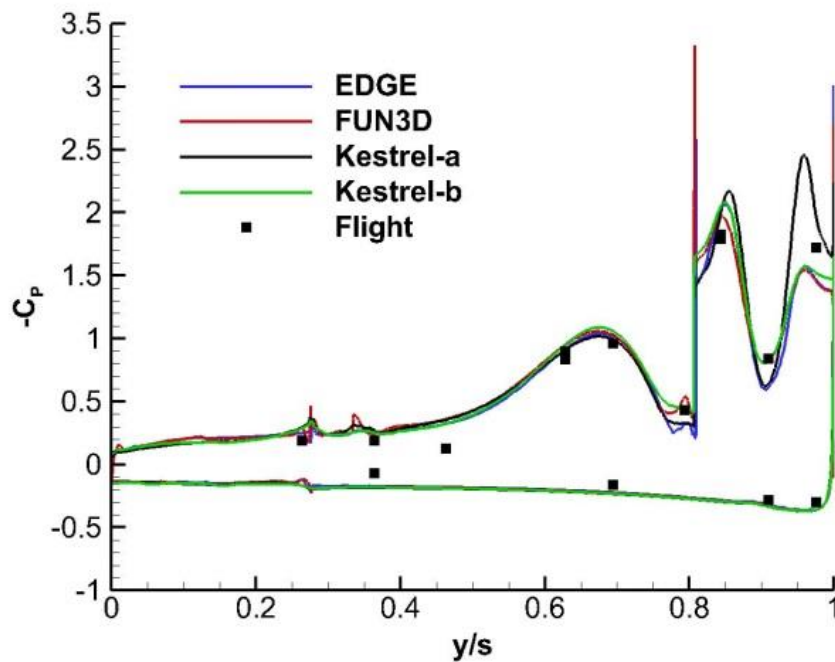American Institute of Aeronautics and Astronautics

a) Mean C_p

b) Mean $\pm$ SD C_p

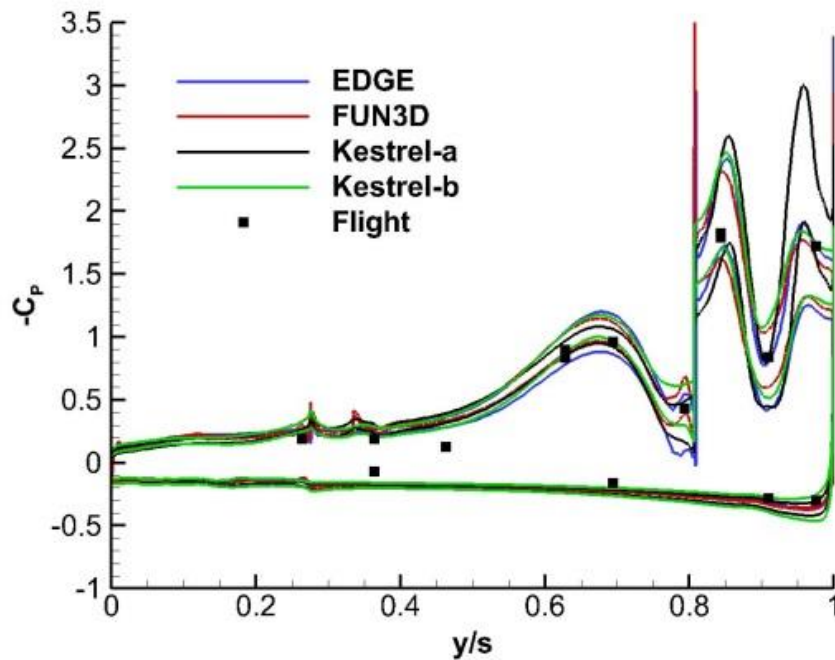**Figure 11. Unsteady surface pressure coefficients, FS-375. FC-25, M = 0.242, Re_{cref} = 32.22 x 10^6, α = 19.84°.**
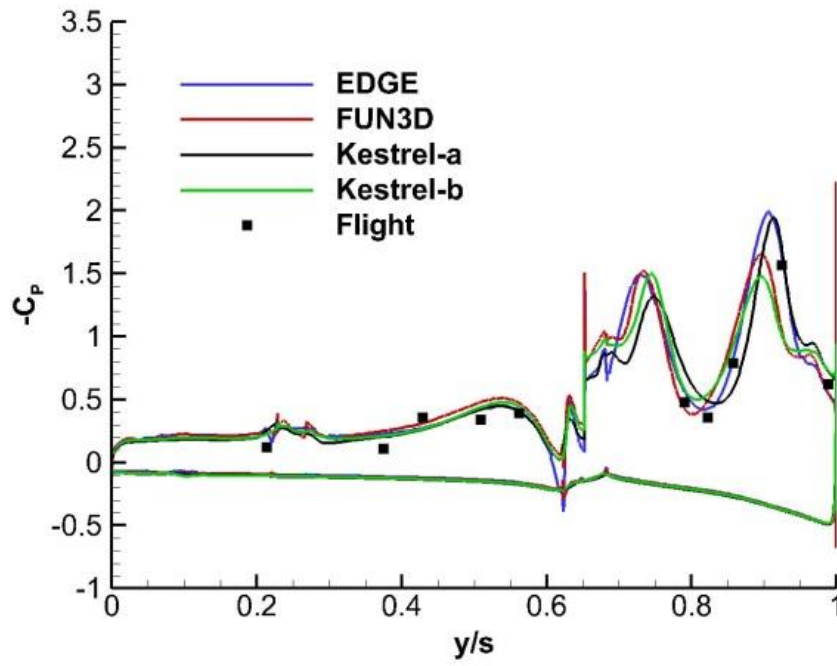
a) Mean C_p

b) Mean ± SD C_p

Figure 12. Unsteady surface pressure coefficients, FS-407.5. FC-25, M = 0.242, Re$_{cref}$ = 32.22 x 10^6, α = 19.84^o.

a) Mean C_p
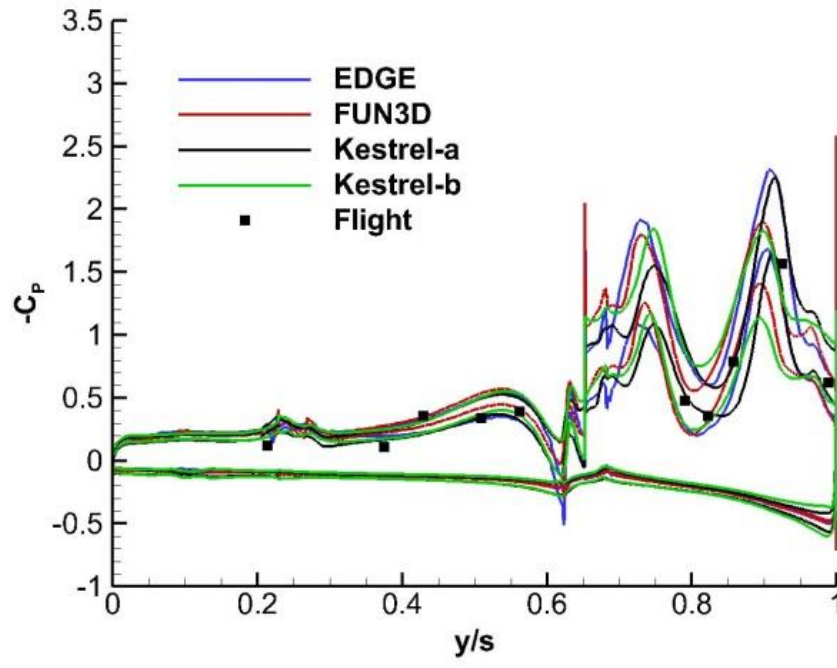

b) Mean ± SD C_p

Figure 13. Unsteady surface pressure coefficients, FS-450. FC-25, M = 0.242, Re_{cref} = 32.22 x 10^6, α = 19.84°.

2. Chordwise Butt Lines

The same approach to pressure analysis will be used for the chordwise butt-line pressure distributions. Results will be shown for BL- 55, 70, 80, 95, 153.5, and 184.5.

Results are first presented in **Figure 14** for BL-55. At this station, the leading edge is still on the s-blend portion of the planform. With the exception of the EDGE solution, the mean pressure coefficient solutions are close to each other. There appears to be a double suction peak near the leading edge in both the CFD and the measurements. This may be due to the primary and a strong secondary vortical flow, although more analysis would be needed to confirm this conjecture. Vortical flows are more easily interpreted in cross-flow planes due to slender wing similarity principles, and the s-blend introduces its own variations to the vortices (see Hitzel[23] [2014]). Unsteady effects are prevalent on the first 0.30 chord and give the appearance of containing the experimental measurements.

Results are next presented in **Figure 15** for BL-70. At this station, the s-blend has just completed to match the 70°-swept inboard portion of the wing. There is much more scatter among the computations in the regions of the secondary and primary vortices. Unsteady effects are noted over the forward 0.40 chord, and the magnitude of unsteadiness differs among the methods.

Results are presented in **Figure 16** for BL-80. This station is within the 70°-swept inboard portion of the wing. Now clear secondary-vortex and primary-vortex footprints can be observed in the mean pressures, Figure 16a, and the higher secondary-vortex suction pressure from the Kestrel-a simulation can also be observed. Unsteady effects are now observed over the full chord of the airfoil. As the butt line stations move outboard, the aft portions are approaching the vortex breakdown region of the wing discussed in the flowfield and fuselage station analyses. The increased aft unsteadiness is, thus, consistent with the prior vortex flow analyses.

Results are presented in **Figure 17** for BL-95. The leading edge at this butt line station is slightly upstream of the leading edge for the first fuselage station analyzed, FS-300. Much of this spanstation falls under the secondary vortex, which accounts for the flat mean pressures on the forward 0.25 chord. The primary vortex suction peak is evident, and the simulations are in fair agreement with each other and the experimental data. Once again full chord unsteady effects are seen, Figure 17b, for much of the same reasoning as discussed with BL-80. It is also noted that, to the extent the mean pressure coefficient predictions differ with the measurements (Figure 17a), these differences

are fully contained by the unsteady effects as shown in Figure 17b. BL-95 is the last analysis station for the inner, 70°-swept portion of the wing.

Results are presented in **Figure 18** for BL-153.5. The station is located at slightly less than midspan of the outer, 50°-swept wing panel. This station has the very complex vortical flows discussed earlier with Figure 12 (FS-407.5). Looking at the mean pressure coefficients, the Kestrel-a results show the stronger primary leading-edge vortex as discussed earlier with Figure 12; they differ the most from the other simulations. All of the simulations differ from the experimental measurements. All of the simulations also show significant unsteady effects (Figure 18b), and here it is noted that the collective unsteady simulations contain the experimental measurements. This station has some of the most complex and unsteady vortical flows, and it is at least plausible, in light of Figure 18b, that the lack of correlation shown in Figure 18a could be associated with unsteady vortex flow effects. This point will be further discussed later in this section.

Results are presented in **Figure 19** for BL-184.5. This is the farthest outboard station on the outer wing panel, and is close to the tip-missile rail system. The mean pressures on the upper surface are quite flat with a possible suction effect near 0.45 chord; this could be due to the outer-panel leading-edge vortex. Once again, however, the unsteady effects shown in Figure 19b fully contain the data, so caution is needed in interpreting the small increments in the mean pressure coefficients between simulation and experiment.
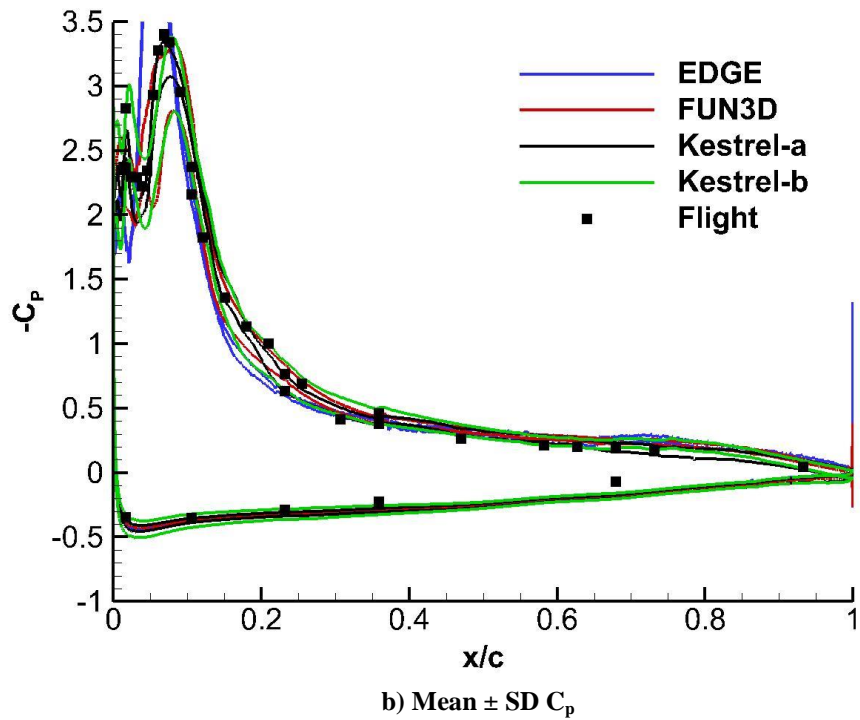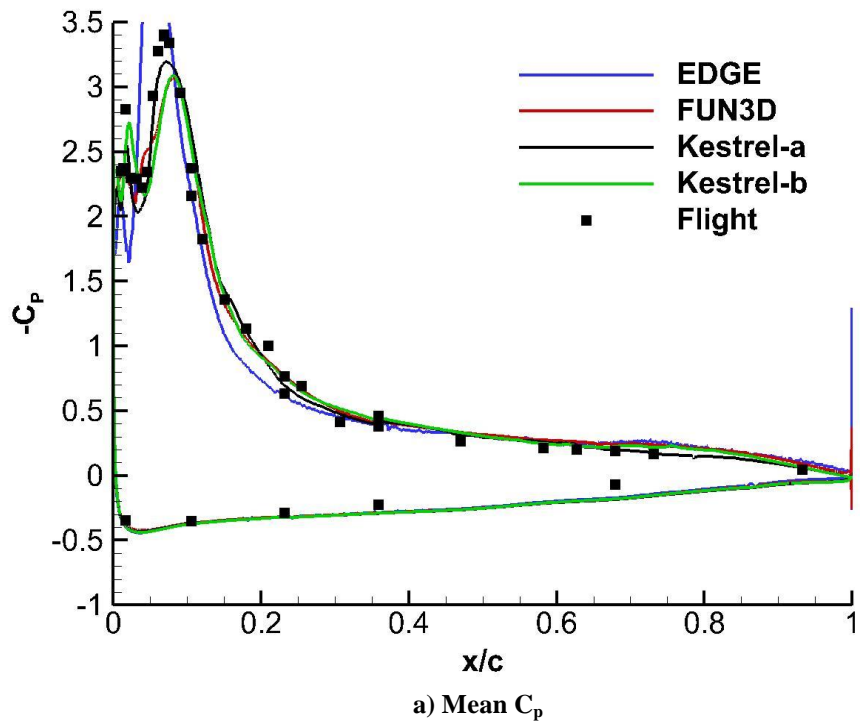
American Institute of Aeronautics and Astronautics

a) Mean C_p

b) Mean ± SD C_p

Figure 14. Unsteady surface pressure coefficients, BL-55. FC-25, M = 0.242, Re_{cref} = 32.22 x 10^6, α = 19.84°.

American Institute of Aeronautics and Astronautics

a) Mean C$_p$

b) Mean ± SD C$_p$

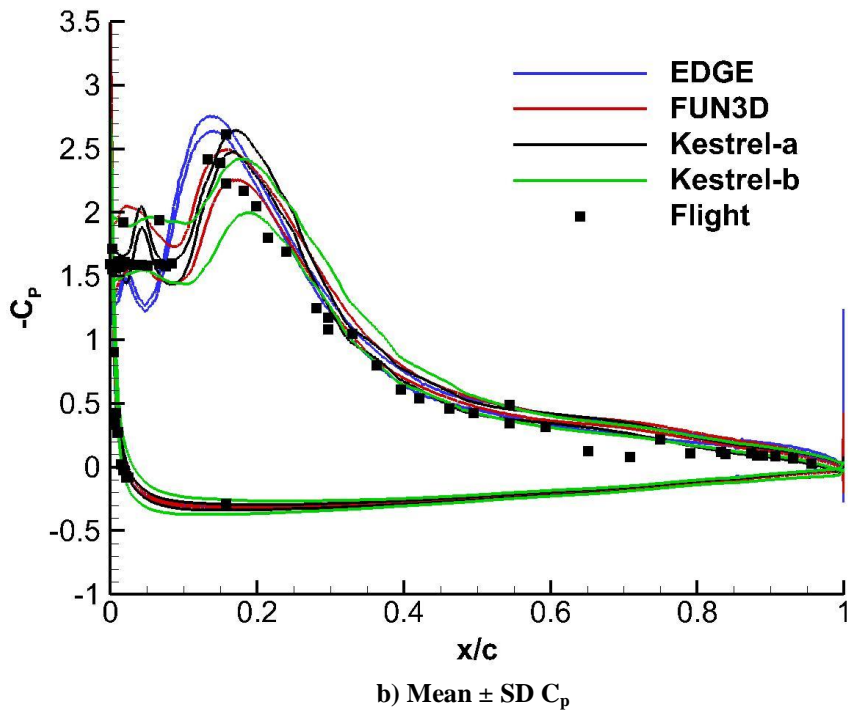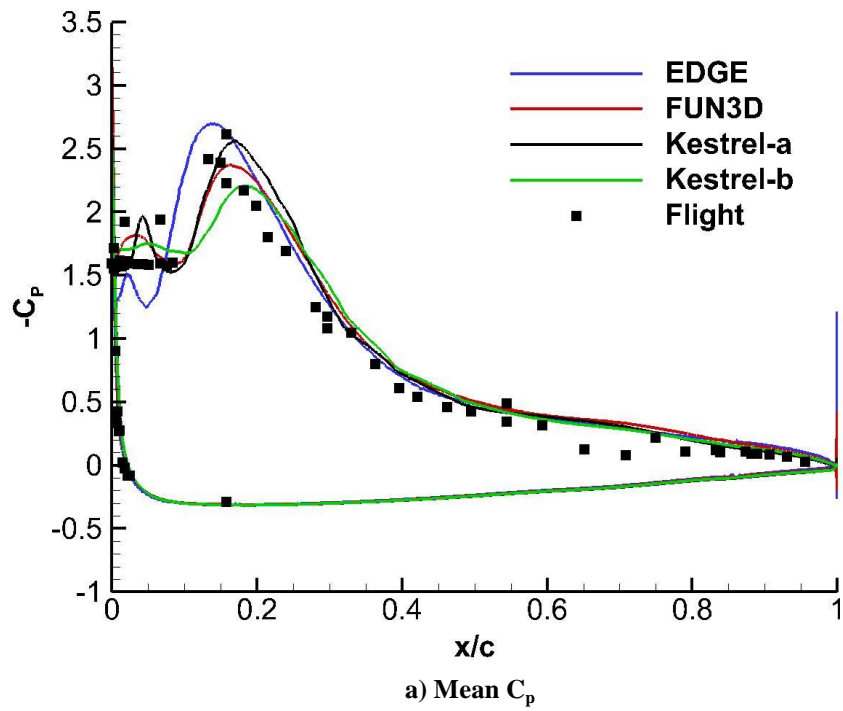**Figure 15. Unsteady surface pressure coefficients, BL-70. FC-25, M = 0.242, Re$_{cref}$ = 32.22 x 10^6, α = 19.84^o.**
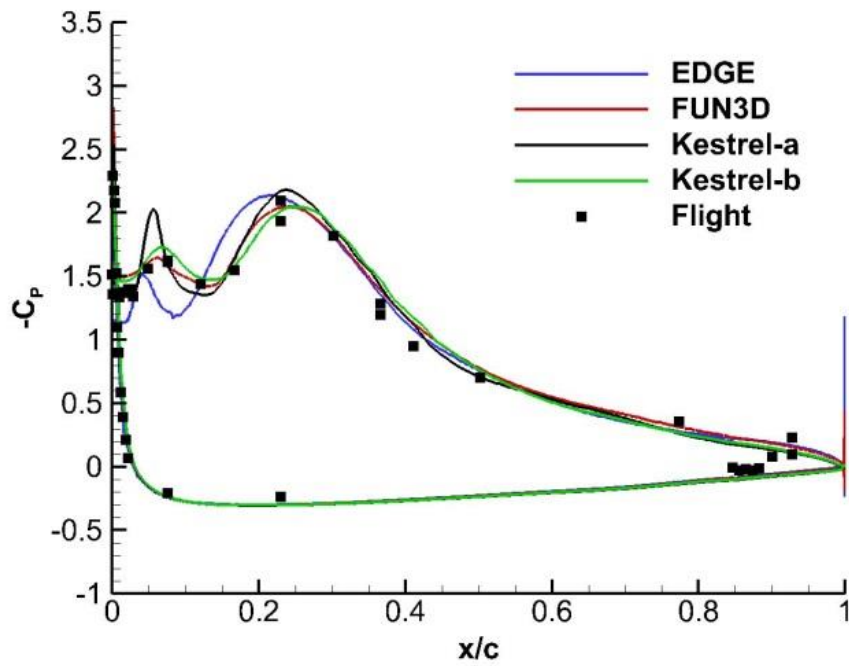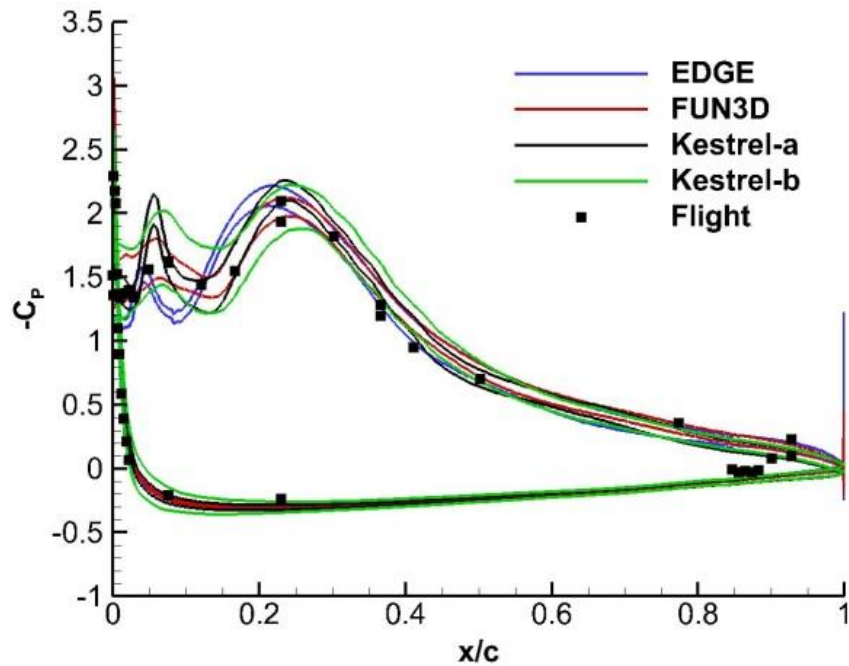
a) Mean C_p

b) Mean ± SD C_p

Figure 16. Unsteady surface pressure coefficients, BL-80. FC-25, M = 0.242, Re_{cref} = 32.22 x 10^6, α = 19.84°.
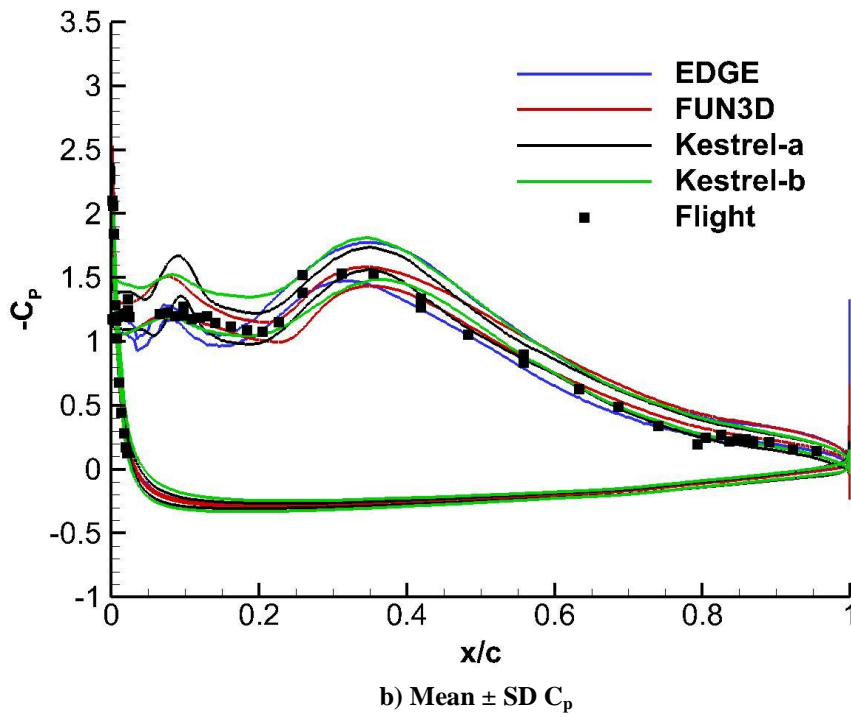
a) Mean C_p

b) Mean ± SD C_p

Figure 17. Unsteady surface pressure coefficients, BL- 95. FC-25, M = 0.242, Re_{cref} = 32.22 x 10^6, α = 19.84^o.

American Institute of Aeronautics and Astronautics

a) Mean C_p

b) Mean ± SD C_p

Figure 18. Unsteady surface pressure coefficients, BL-153.5. FC-25, M = 0.242, Re_{cref} = 32.22 x 10^6, α = 19.84°.

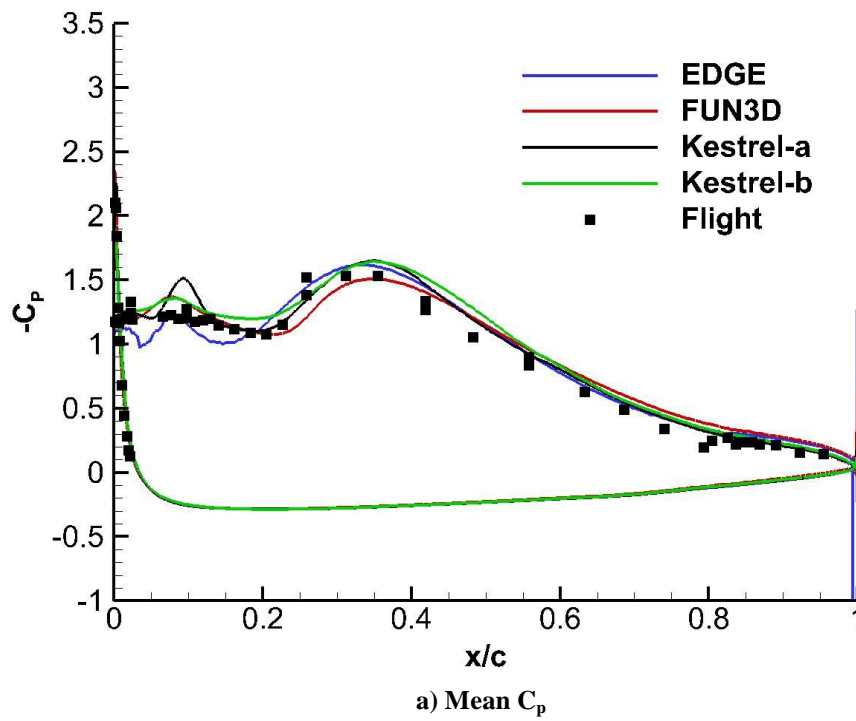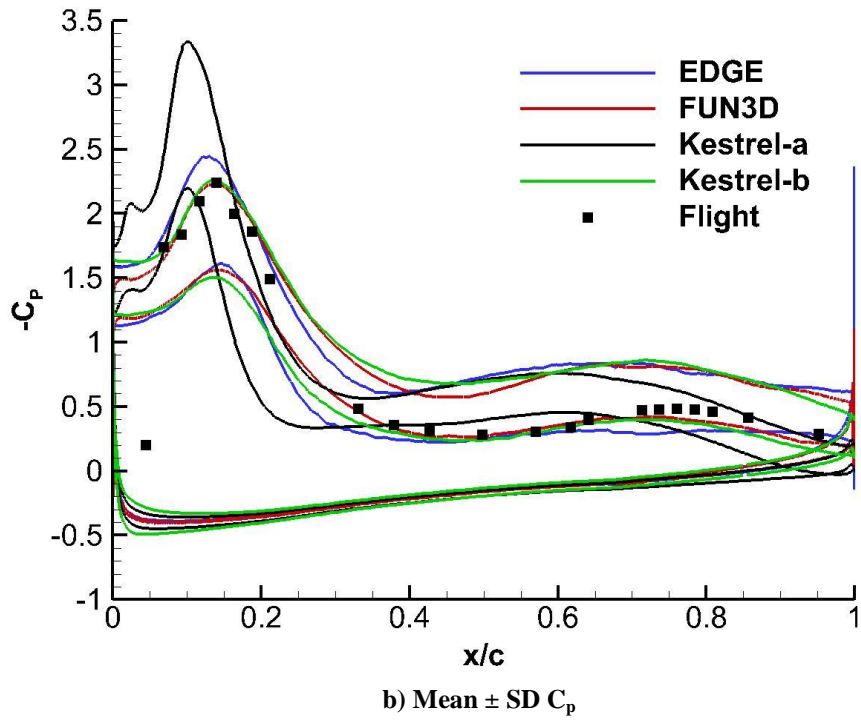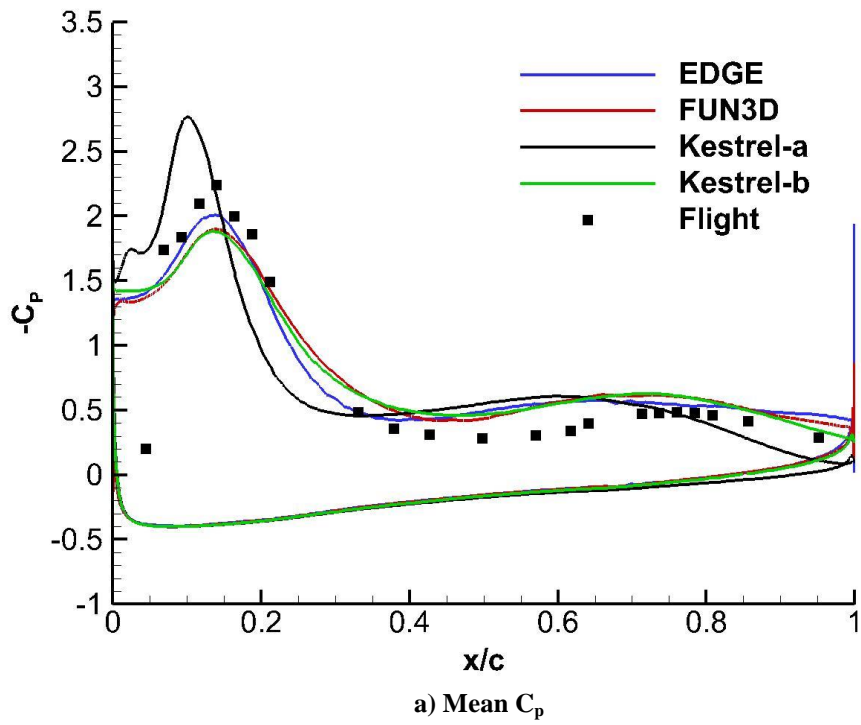a) Mean C_p

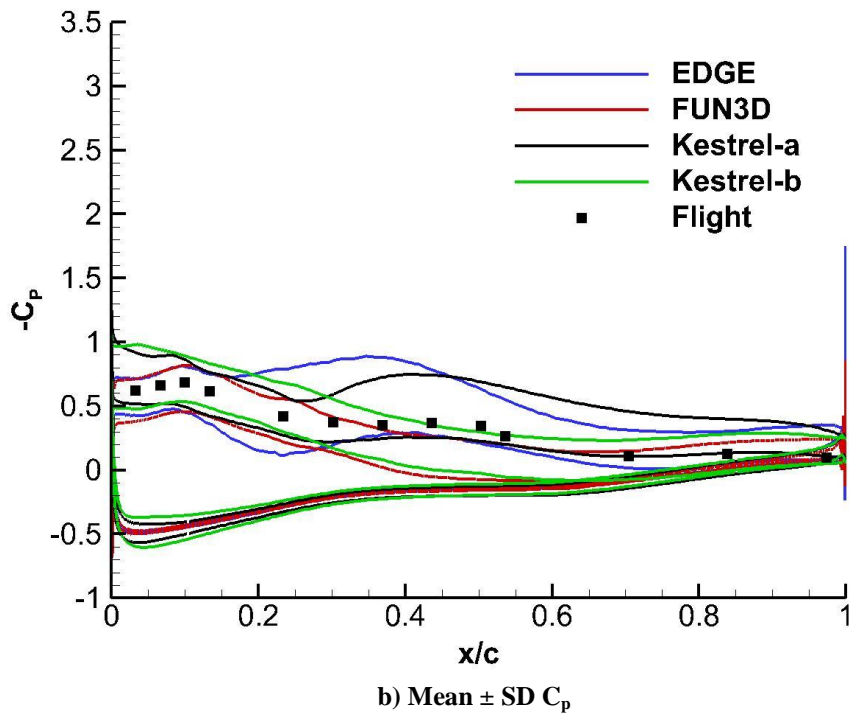

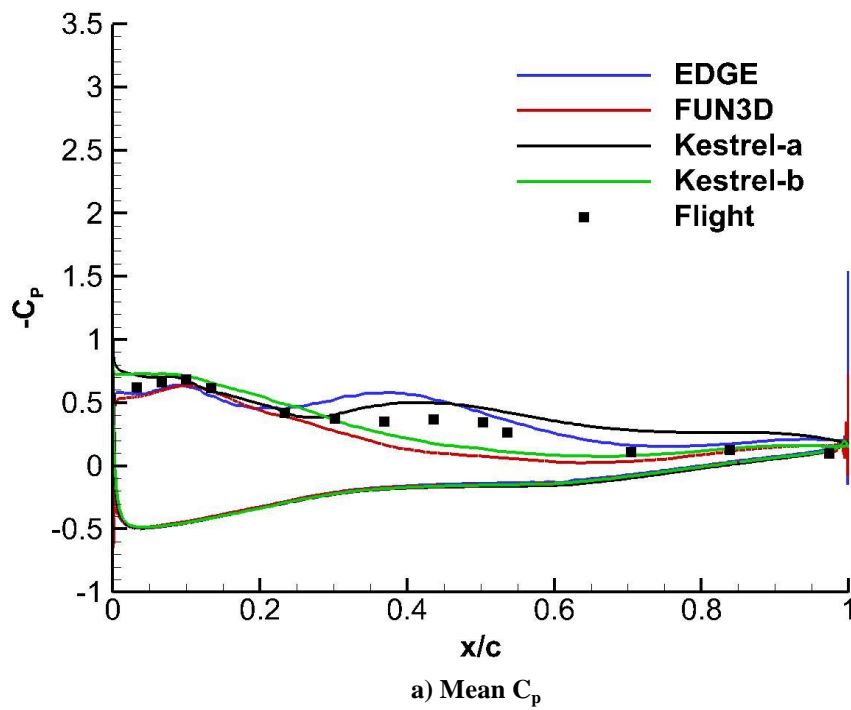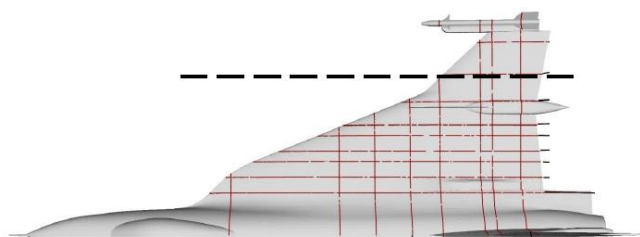b) Mean ± SD C_p

Figure 19. Unsteady surface pressure coefficients, BL-184.5. FC-25, M = 0.242, Re_{cref} = 32.22 x 10^6, α = 19.84°.

American Institute of Aeronautics and Astronautics

The unsteady vortex flow effects discussed with Figure 18 (BL-153.5) are now further addressed with **Figure 20**. Figure 20a illustrates BL-153.5, Figure 20b repeats the mean ± SD surface pressures of Figure 18b, for convenience, and Figure 20c is taken from Lofthouse and Cummings[6] [2015]. All the computations in Figure 20c are from Kestrel-b, and they include the mean pressure coefficient, the mean ± SD pressure coefficients, and the minimum and maximum pressure coefficients from the analysis window of that simulation. Experimental results are also included.

The mean ± SD results from EDGE, FUN3D and Kestrel-b in Figure 20b bracket the data as mentioned before. In addition, the mean + SD data follow the trends on the forward portion of the wing, while the mean − SD data follow the trend of the data for the remainder of the wing. The Kestrel-a results have a stronger leading-edge vortex, which account for the higher suction peaks in Figure 20b.
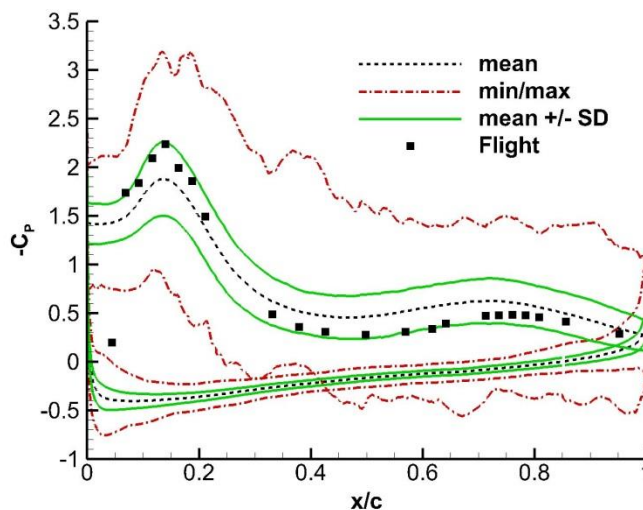
The Kestrel-b results are also used to further illustrate the magnitude of

a) BL 153.5
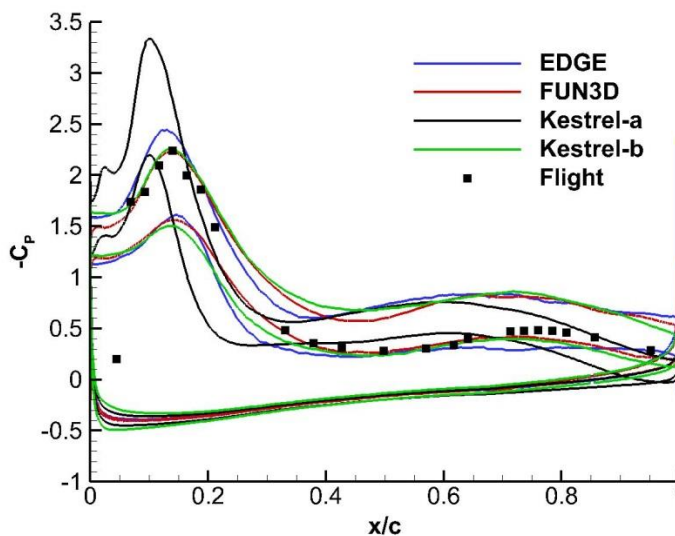
b) Mean ± SD C_p

c) Unsteady surface C_p, Kestrel-b.

Figure 20. Unsteady pressure coefficients, BL-153.5. FC-25, M = 0.242, Re_{cref} = 32.22 x 10^6, α = 19.84°.

unsteady pressure variations in Figure 20c. The min/max results show the broad range of pressure excursions from the mean result for this simulation. Similar unsteady pressure excursions were shown by Morton and McDaniel[8] [2015] for the Kestrel-a simulations.

These results of Figure 20, more than any other, clearly indicate how unsteady the outer wing panel flow could be. The differences between the simulation mean-flow pressure coefficients and the experimental pressure coefficients (see Figure 18a) are very small as compared to the magnitude of the unsteady pressure excursions. This would also mean the details of the measurements would warrant further analysis in light of recording pressures with some form of steady-flow measurement technology in what could very well be such an unsteady flow environment.

It must also be observed that the vortical contributions to this unsteady flow environment are exceptionally complex, not necessarily well understood, and most likely not well predicted. Some vortex phenomena that could contribute to this flow would include vortex breakdown, vortex/vortex interactions, secondary vortex effects, and vortex hysteresis. Few of these phenomena are well predicted in isolation, and for the F-16XL, these are all occurring in an interacting and unsteady environment. It is likely that new experiments will be needed to isolate these phenomena and work toward improved predictive capabilities.

C. Off-body Flows

The unsteady flowfields were further examined by sampling the off-body flow. Original work was performed by Hitzel[7] [2015], and his original 54 points (semispan) were downselected to 15 points (semispan) by Morton and McDaniel[8] [2015] for comparison purposes across the methods. These points are shown in **Figure 21**. One set of points was focused inboard and upstream in the vicinity of the wing apex. These were positioned to sample the leading-edge vortex from the 70°-swept leading edge. The second set of points was focused downstream on the outer panel near the leading edge. These were positioned to sample the leading-edge vortex from the outboard 50°-swept leading edge. Five partners contributed results for the comparison analysis. It is noteworthy that Hitzel's points cover the full span (108 points); this was done to support the analysis of flows at sideslip conditions. The reader is referred to Hitzel's work[7] for very detailed analyses of the off-body flows.
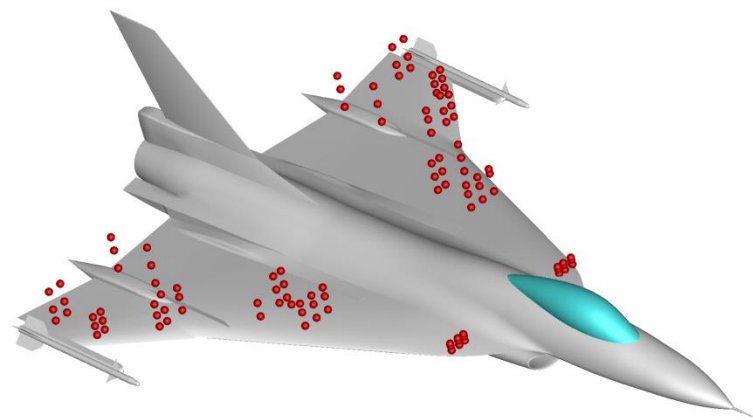
a) Field analysis points, Hitzel[7] [2015]
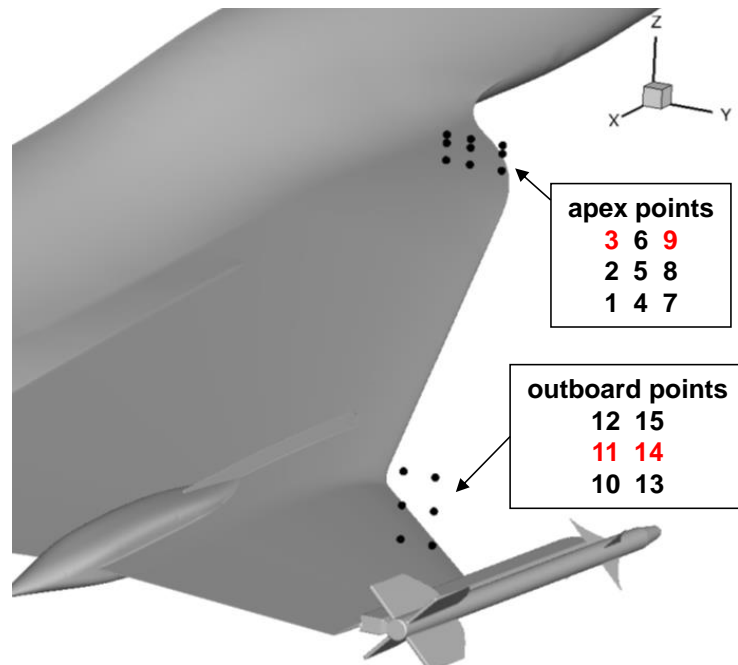
b) Downselected points, Morton and McDaniel[8] [2015]

Figure 21. Flowfield analysis points.

Results were further downselected to points 3, 9, 11, and 14, as indicated in Figure 20b, for the present analysis, and flowfield results are shown in **Figure 22**. The results chosen for this analysis are Sound Pressure Level (SPL), measured in decibels (dB). Looking at the two upstream points, Figure 22a and 22b, a number of discrete tones are predicted with three of the five methods. Details differ for the tones among the results, and this may be associated with the relative position of the leading-edge vortex in the solutions. The points are fixed in space, so they will be

positioned slightly differently relative to the local vortical flow. The tones could be associated with vortical substructures, although details would require further analysis. In addition, differing grid resolution is likely affecting the results across the methods.

The two downstream points, Figure 22c and 22d, show a broadband distribution sound pressure level, and results from all methods are in reasonable agreement. This broadband characteristic is consistent with the more broken down nature of the vortices.
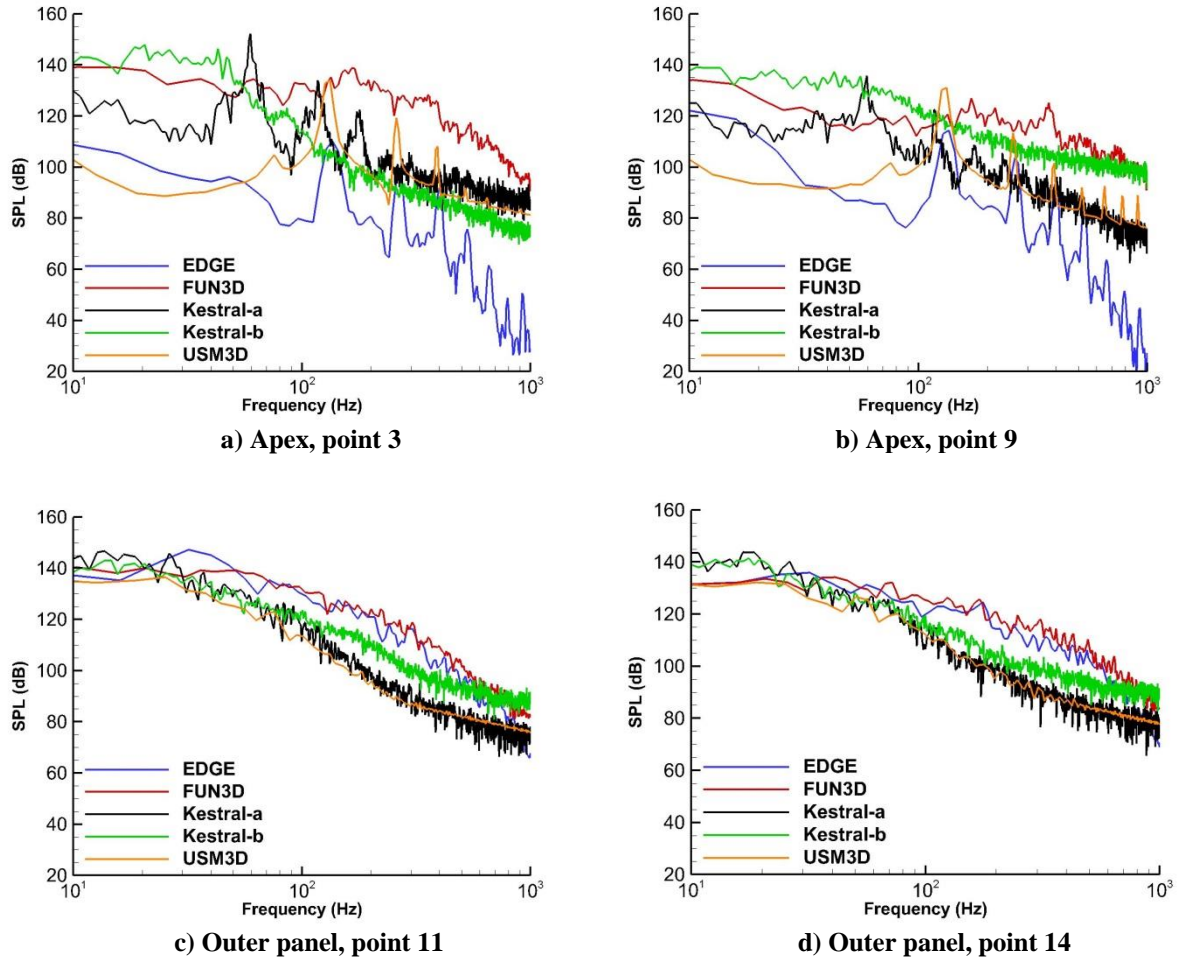

a) Apex, point 3

b) Apex, point 9

c) Outer panel, point 11

d) Outer panel, point 14

Figure 22. Comparison of predicted off-body flow spectra. FC-25, M = 0.242, Re_{cref} = 32.22 x 10^6, α = 19.84°.

D. Forces/moments

    Unsteady forces and moments were also analyzed. Mean and SD variation of the lift, drag and pitching moment coefficients were accumulated over the same time ranges of unsteady analysis reported in Table 3. Five partners contributed results for this analysis.

    Results are shown in **Table 4** and **Figure 23**. The force and moment coefficients are shown in Figure 23 with ± the temporal SD variation about the mean value for each method. In addition, the average of the mean values across the methods is shown. For the lift coefficient, Figure 23a, four of the five methods showed comparable temporal variation. The variation in lift coefficient due to method was much larger than the temporal variations. For the drag coefficient, Figure 23b, all methods showed comparable temporal variation and again the variations due to method were much larger than the temporal variations.

Table 4. Force and Moment Summary. FC-25, M = 0.242, Re_{cref} = 32.22 x 10^6, α = 19.84°.

| Partner | Code | C_L | | C_D | | C_m | | x_{cp}/L_{ref} |
		mean	SD	mean	SD	mean	SD	mean
KTH	EDGE/Hyb0	0.777	0.0070	0.4417	0.0022	-0.0068	0.0036	0.506
NASA LaRC	FUN3D	0.802	0.0054	0.4528	0.0020	-0.0021	0.0025	0.504
NASA LaRC	USM3D	0.751	0.0055	0.4801	0.0018	0.0062	0.0034	0.500
CREATE	Kestrel-a	0.818	0.0088	0.3830	0.0033	0.0076	0.0036	0.499
USAFA	Kestrel-b	0.786	0.0014	0.4600	0.0029	0.0012	0.0052	0.502

    For the pitching moment coefficients, Figure 23c, the variations were small, and the methods each had comparable temporal variations. The moment reference point was the aircraft center of gravity, and since the F-16XL was designed to be neutrally stable, the resultant pitching moments were small. As a second metric, these results were used to determine the center of pressure for each method, normalized by the length of the aircraft (54.16 ft.). The longitudinal moment reference point, normalized by the length of the aircraft, is x_{mrp}/L_{ref} = 0.503, and the variations in center of pressure from the five methods is shown in Figure 23d. The scale is quite expanded, and the variation among the methods is less than 0.7 percent of the aircraft length.
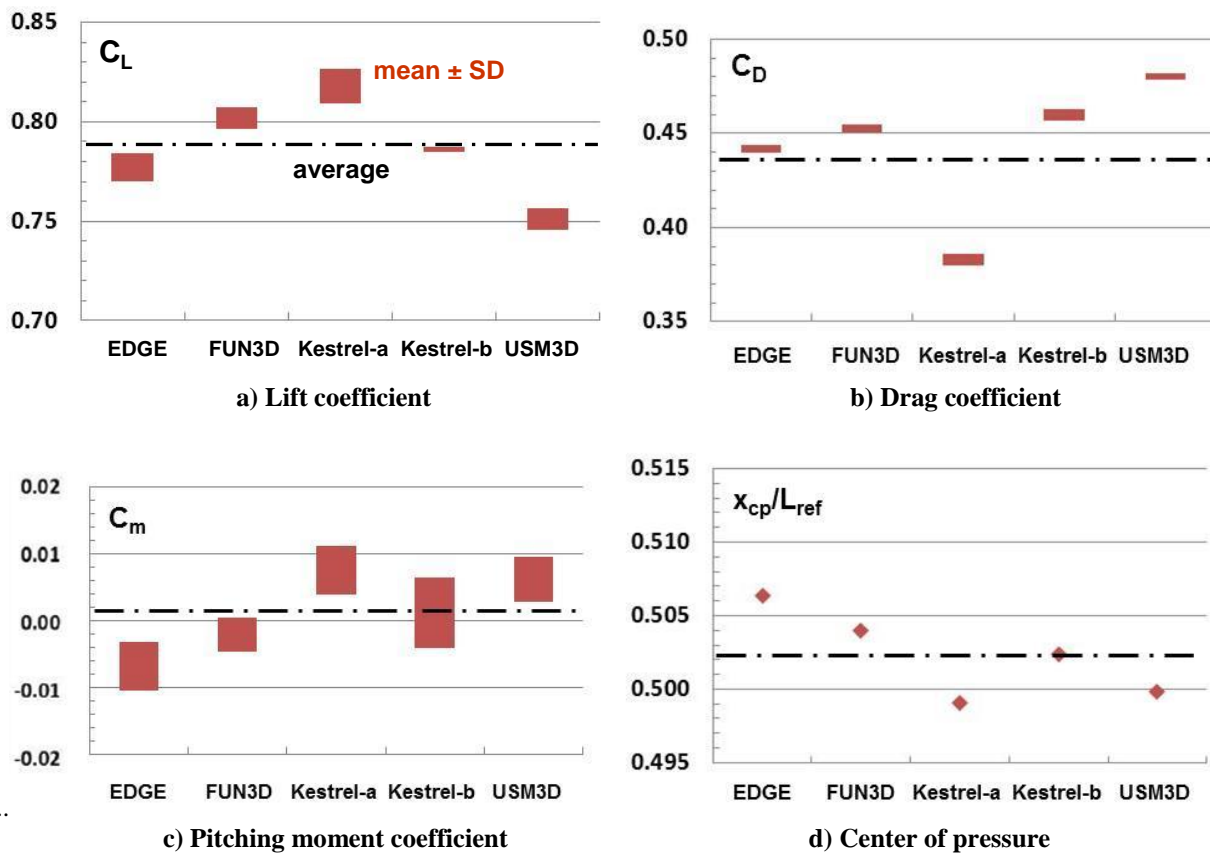
American Institute of Aeronautics and Astronautics

a) Lift coefficient

b) Drag coefficient

c) Pitching moment coefficient

d) Center of pressure

Figure 23. Force and moment properties. FC-25, M = 0.242, Re_{cref} = 32.22 x 10^6, α = 19.84°.

VI.   Concluding Remarks

This study was focused on unsteady aerodynamic assessments with hybrid RANS/LES methods for the F-16XL aircraft at a low-speed, high angle-of-attack condition. Prior studies, with a focus on steady RANS methods, had failed to produce acceptable CFD predictions of the aircraft outer-panel wing properties as compared to flight test.

The new work included six independent assessments, using five hybrid RANS/LES methods. The overall predicted flowfields were compared, and a combination of steady and unsteady analysis was performed for wing pressures, off-body flow properties, and forces and moments. Correlations among the methods, and with unique flight-test measurements were included.

The unsteady simulations demonstrated that the wing outer-panel flow is very unsteady due to a complex suite of vortex flows and interactions. The collective unsteady predictions for the wing outer-panel aerodynamics bound the experimental data, and at least imply that unsteady aerodynamic effects are a significant contributor to the prior discrepancies between flight and (steady RANS) CFD. At other locations, where the flow was predicted to be mostly

steady, the correlation among the simulations and with flight test was good. The predicted unsteady effects also agreed fairly well among the methods. The vortex flows from this study are very rich, and further analysis of the vortical structures and their unsteady attributes is warranted.

The F-16XL flight data have proven to be a valuable forum for assessments of advanced CFD methods to predict slender wing aerodynamics. Many opportunities for CFD assessments are untapped in this database. At the same time, a deeper understanding of the complex unsteady and interacting vortical flows of this study could benefit from new experimentation designed to isolate and quantify these phenomena.

VII. Acknowledgments

VIII. References

[1]Lamar, J. E., Obara, C. J., Fisher, B. D., and Fisher, D. F., "Flight, Wind-Tunnel, and Computational Fluid Dynamics Comparison for Cranked Arrow Wing (F-16XL-1) at Subsonic and Transonic Speeds," NASA TP 2001-210629, Feb 2001.

[2]Lamar, J. E., "Cranked Arrow Wing (F-16XL-1) Flight Flow Physics with CFD Predictions at Subsonic and Transonic Speeds," RTO MP-069, Paper 44, 2003.

[3]Obara, C. J., and Lamar, J. E., "Overview of the Cranked-Arrow Wing Aerodynamics Project International," Journal of Aircraft, Vol. 46, No. 2, 2009, pp. 355–368.

[4]Rizzi, A., Jirásek, A., Lamar, J. E., Crippa, S., Badcock, K. J., Boelens, O. J., "Lessons Learned from Numerical Simulations of the F-16XL Aircraft at Flight Conditions," Journal of Aircraft, Vol. 46, No. 2, 2009, pp. 423–441.

[5]Rizzi, A., and Luckring, J. M., "What was Learned in Predicting Slender Airframe Aerodynamics with the F16-XL Aircraft", AIAA 2014-0759, Jan 2014.

[6]Lofthouse, A. J., and Cummings, R. M., "Numerical Simulation of the F-16XL at Full-Scale Flight Test Conditions Using Delayed Detached-Eddy Simulation," AIAA 2015-2875, June 2015.

[7]Hitzel, S. M. "Free Flight High AoA Flows Simulations at Sub- and Transonic Speeds – F-16 XL (CAWAPI-3),"AIAA 2015-2871, June 2015.

[8]Morton, S. A., and McDaniel, D. R., "Numerical Simulation of the F-16XL at Full-Scale Flight Test Conditions Using a Near-Body Off-Body CFD Approach," AIAA 2015-2873, June 2015.

[9]Park, M. A., Elmiligui, A., and Abdol-Hamid, K., S., "F-16XL Hybrid Reynolds-averaged Navier-Stokes/Large Eddy Simulation on Unstructured Grids," AIAA 2015-2872, June 2015.

[10]Rizzi, A., Tomac, M., and Jirásek, A., "Hybrid RANS-LES Simulations of F-16XL Aircraft in Low-Speed High-Alpha Flight," AIAA 2015-2874, June 2015.

[11] Elmiligui, A., Abdol-Hamid, K., and Parlette, E. B., "Detached Eddy Simulation for the F-16XL Aircraft Configuration" AIAA 2015-1496, 2015.

[12]Hillaker, H. J., "F-16XL Flight Test Program Overview," AIAA Paper 83-2730, Nov. 1983.

[13]Talty, P. K., and Caughlin, D. J., "F-16XL Demonstrates New Capabilities in Flight Test at Edwards Air Force Base," Journal of Aircraft, Vol. 25, No. 3, Mar. 1988, pp. 206–215.

[14] Gerhold, T., "Overview of the Hybrid RANS Code TAU," in N. Kroll, J. Fassbender (Eds.) MEGAFLOW – Numerical Flow Simulations for Aircraft, NNFM, Vol. 89, Berlin, 2005, pp. 81-92.

[15]Eliasson, P., Edge, a Navier-Stokes solver for unstructured grids. In Finite Volumes for Complex Applications III, pages 527-534, June 2002.

[16]Peng, S.H. Hybrid RANS-LES Modeling Based on Zero- and One-Equation Models for Turbulent Flow Simulation. In Turbulence and Shear Flow Phenomena, pages 1159-1164, June 2005.

[17]Biedron, R. T., Carlson, J.-R., Derlaga, J. M., Gnoffo, P. A., Hammond, D. P., Jones, W. T., Kleb, B., Lee-Rausch, E. M., Nielsen, E. J., Park, M. A., Rumsey, C. L., Thomas, J. L., and Wood, W. A., "FUN3D Manual: 12.7," NASA TM-2015-218761, Langley Research Center, May 2015.

[18]Frink, N. T., "Tetrahedral Unstructured Navier-Stokes Method for Turbulent Flow," AIAA Journal, Vol. 36, No. 11, Nov. 1998, pp. 1975-1982.

[19]Frink, N. T., Pirzadeh, S. Z., Parikh, P., Pandya, M. J., and Bhat, M. K., "The NASA Tetrahedral Unstructured Software System," The Aeronautical Journal, Vol. 104, No. 1040, Oct. 2000, pp. 491-499.

[20]Post, D. E., "Highlights of the CREATE Program," Proceedings of the DoD HPCMP User Group Conference, Schaumburg, IL, 2010.

[21]Roth, G. L., Morton, S. A., and Brooks, G. P., "Integrating CREATE-AV Products DaVinci and Kestrel: Experiences and Lessons Learned," AIAA Paper 2012-1063, 50th AIAA Aerospace Sciences Meeting, Nashville, TN, Jan. 2012.

[22]Morton, S. A., McDaniel, D. R., Sears, D. R., Tillman, B., and Tuckey, T. R., "Kestrel: A Fixed Wing Virtual Aircraft Product of the CREATE Program," AIAA Paper 2009-0338, 47th AIAA Aerospace Sciences Meeting, Orlando, FL, Jan. 2009.

[23]Hitzel, S., "Vortex Flows of the F-16XL Configuration - CAWAPI-II Free-Flight Simulations," AIAA 2014-0758, Jan 2014.

[24]Elmiligui, A., Abdol-Hamid, K., Cavallo, P. A., and Parlette, E. B., "Vortex Numerical Simulations for the F-16XL Aircraft Configuration," AIAA 2014-0756, Jan 2014.